Chapter 7
Mimicking SOD, Why and How: Bio-Inspired Manganese Complexes as SOD Mimic

Clotilde Policar

Abbreviations

ACN	Acetonitrile
ATP	Adenosine triphosphate
ALS	Amyotrophic lateral sclerosis
CYP450	Cytochrome P450
CD	Cyclodextrin
CN	Coordination number
DNA	Deoxyribonucleic acid
DMSO	Dimethylsulfoxide
DMF	*N,N*-Dimethylformamide
EPR	Electron paramagnetic resonance
EWG	Electron-withdrawing group
GSH	Glutathione
HAS	Human serum albumin
LFSE	Ligand-field stabilization energy
MMO	Methane monooxygenase
NBT	Nitroblue tetrazolium
PCET	Proton-coupled electron transfer
PROS	Partially reduced oxygen species
ROS	Reactive oxygen species
RNS	Reactive nitrogen species
SOD	Superoxide dismutase

C. Policar (✉)
Département de Chimie, École Normale Supérieure-PSL Research University, Sorbonne Universités, UPMC Univ Paris 06, CNRS, Laboratoire des BioMolécules, UMR 7203, 24, rue Lhomond, Paris 75005, France
e-mail: clotilde.policar@ens.fr

I. Batinić-Haberle et al. (eds.), *Redox-Active Therapeutics*,
Oxidative Stress in Applied Basic Research and Clinical Practice,
DOI 10.1007/978-3-319-30705-3_7

SOR	Superoxide reductase
UV-vis.	UV-visible spectroscopy
WT	Wild type

7.1 Mimicking Manganese Superoxide Dismutases: Why and How?

[Naturam] si sequemur ducem, numquam aberrabimus, Cicero, *De officiis*, I, 100
Let Nature guide us: we shall never get lost

Superoxide dismutases (SODs) are crucial proteins for protecting cells from superoxide, a reactive species derived from dioxygen by one-electron reduction. SODs catalyze the dismutation of superoxide, resulting in a tight control of its concentration in biological environments. Superoxide is a metastable anion endowed with both signaling functions and toxic properties, valuable for fighting against pathogens. Superoxide can be harmful leading to molecular modifications, which disturb endogenous functions of biomolecules. Oxidative stress reflects an imbalance between the continuous production of reactive oxygen species (ROS) and the antioxidant protective pathways, and is associated with a wide range of physiopathological conditions, including aging. SODs are remarkably efficient proteins that have elicited strong interests for many years. Indeed, besides the biological role of SOD in controlling oxidative stress conditions, understanding their physicochemical parameters, selected by evolution and responsible for their amazing efficiencies, is of fundamental interest and can also serve as a useful and effective guideline for chemists aiming at developing antioxidant derivatives for therapeutic applications against oxidative stress. This chapter focuses on the SOD physicochemical parameters that are useful for chemical design of low-molecular-weight complexes displaying superoxide scavenging activity. Nature is an endless source of both inspiration and challenges for chemists, and in turn, chemical modeling can help in deciphering underlying physicochemical characteristics determining bioactivity. Inspiration from natural systems and processes, providing their mechanisms have been dissected with care, can pave the way to efficient and original systems. The development of low-molecular-weight SOD mimics constitutes a shining example of this fertile interplay with Nature.

7.2 Dioxygen and Superoxide Dismutases

7.2.1 Dioxygen and Oxidative Stress

Dioxygen is necessary for aerobic life. Its concentration rose on Earth as a result of oxygenic photosynthesis that appeared in cyanobacteria about 2.5 billion years ago. This process enables the efficient retrieving of light energy for the synthesis of ATP, and ultimately organic sugars, and releases O_2 as a by-product. Rising concentration

in dioxygen initiated a profound modification of the redox state on Earth, going from a reducing environment, still roughly found in the interior of cells, to an oxidant environment. In a certain sense, dioxygen can be considered as the first chemical pollutant and held responsible for an event called the *Oxygen Catastrophe* or the *Great Oxidation Event* [1, 2]. The increase in its concentration was associated with strong variations in the chemical environment on Earth: the greenhouse methane gas disappeared, with a fast decrease in temperature [2], oxidation of metal ions with drastic modifications in their solubility and bioavailability occurred [3], etc. The appearance of dioxygen triggered an increase in molecular diversity by opening the possibility of oxygen incorporation into organic molecules through new metabolic pathways. However, because of its triplet spin-state ($S=1$) resulting from its two-unpaired electron, diradical ground state nature, dioxygen is not very reactive with organic molecules ($S=0$, singlet, with all paired electrons): the incorporation of an oxygen atom into a C–H bond, leading to a C–OH moiety for instance, corresponds to the creation of new covalent bonds associated with a spin-flip from the $S=1$ diradical dioxygen species, which is energetically costly with a high activation barrier [4]. Hence, to be used by biological systems, dioxygen needs to be activated, which mainly occurs through reductive pathways as in cytochromes P450 (CYP450) or methane monooxygenase (MMO), etc. [5, 6]. Dioxygen can take up four electrons leading to water or can be sequentially reduced into superoxide ($O_2^{\bullet -}$), hydrogen peroxide (H_2O_2) or hydroxyl radical ($HO^{\bullet}$) and then H_2O (see Fig. 7.1). The partially reduced species—superoxide, hydrogen peroxide, and hydroxyl radical—are much more reactive than dioxygen itself, with no spin-state kinetic barrier for the reaction with singlet molecules, and hence are called *reactive oxygen species* (ROS) or sometimes, to point out their reduced nature, *partially reduced oxygen species* (PROS) [7]; in this chapter the more commonly used acronym ROS will be used. They are continuously produced in biological systems by endogenous mechanisms. Mitochondrial respiration, the reverse process of photosynthesis, consists of the four-electron reduction of dioxygen into water (Fig. 7.1) and results in a flow of ROS when the four-electron transfer is decoupled, that is, not performed in a single step. This decoupling leads to an incomplete reduction of dioxygen and about 1–3 % of the dioxygen processed by the mitochondria leaks as superoxide [8, 9].

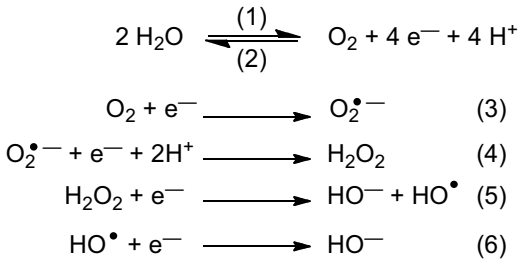

Fig. 7.1 Oxidation of water and reduction of dioxygen. Reduction cascade of O_2 leading to reactive oxygen species ROS. Note that superoxide can be labeled O_2^- or $O_2^{\bullet -}$ to emphasize its radical nature, as dioxygen could be labeled O_2 or $O_2^{\bullet\bullet}$ to indicate its diradical nature. In the main text, we have chosen to use $O_2^{\bullet -}$

Because of their reactivity, ROS can damage endogenous components. The hydroxyl radical $HO^{\bullet}$ is the most reactive and deleterious species in the dioxygen-reduction cascade. $HO^{\bullet}$ initiates radical production through hydrogen abstraction from any R–H molecule with a kinetics close to the diffusion limit, i.e., the first collision with another molecule being reactive-efficient. Superoxide ($O_2^{\bullet -}$) and hydrogen peroxide (H_2O_2) are less reactive but superoxide is known to abstract hydrogen from DNA (DNA nicking) [10, 11], to deactivate radical proteins, such as ribonucleotide reductase, to initiate and also terminate lipid peroxidation [12]. One of the main biological effects of superoxide is the inhibition of iron-sulfur proteins, such as 6-phosphogluconate-dehydratase [13] or aconitase [14, 15], by the destruction of their metallic clusters. This process releases Fe^{II} that may in turn participate in the production of $HO^{\bullet}$ through the Fenton reaction involving H_2O_2 (see Fig. 7.2). This reaction corresponds to the reduction of H_2O_2 into HO^- with the release of $HO^{\bullet}$—note that the oxygen atoms in $HO^{\bullet}$ and H_2O_2 are at the same redox state—and oxidation of Fe^{II} into Fe^{III}. Cu^{I} is able to perform a similar reaction, whereas most of Mn ions, having higher redox potential, are not [9, 16–18]. The concentration of Cu^{I} and Fe^{II} in biological media is tightly controlled and most of iron is coordinated by biomolecules or precipitated within ferritin [19]. This process would not be of much significance if Cu^{I} or Fe^{II} ions were not regenerated, which is made possible by superoxide or other cellular reductants, which may cycle Fe^{III} back to Fe^{II} or Cu^{II} to Cu^{I} (see reaction [8]) leading to the Haber–Weiss reaction (see Fig. 7.2).

But ROS are also useful species. Low levels of ROS are necessary for a variety of cellular processes, including cell adhesion, cell growth and differentiation, or intracellular signaling [20]. In addition, biological systems take advantage of ROS to fight against pathogens. Indeed, macrophages and other immune cells produce high extracellular flows and high intra-phagosome concentrations of ROS to kill infectious agents through oxidative damage [21]. Last, but not least, it has been proposed that the ROS-induced chemical stress on biomolecules, e.g., DNA and proteins, provided an essential source of chemical diversity that enabled adaptation and chemical evolution at the origins of life [22].

In living organisms, efficient pathways to finely tune the concentrations of superoxide and hydrogen peroxide have evolved to protect endogenous components against oxidative damage and to control ROS concentrations to appropriate levels. Such

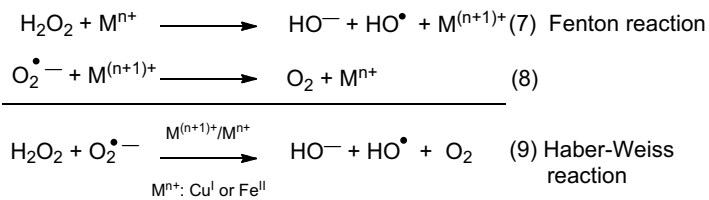

Fig. 7.2 Fenton and Haber Weiss reactions: oxidation of low-oxidation state metal ion by hydrogen peroxide and cycling back to low-oxidation state with superoxide. Note that in biological systems, other reductants can be involved in this reduction

pathways can involve stoichiometric antioxidants (e.g., vitamins E and C, and GSH) or redox enzymes, such as catalase, glutathione peroxidase, superoxide dismutases (SODs), and superoxide reductases (SORs); SODs are the focus of this chapter. Oxidative stress arises when these protective pathways are imbalanced by an increase in ROS flow or a decrease in protective enzymes expression or activity. This leads to a wide range of physiopathological processes, including aging, arthritis, stroke, neurodegenerative diseases (Parkinson and Alzheimer diseases), amyotrophic lateral sclerosis (ALS), cancer, or inflammation [22–26].

7.2.2 *Superoxide Dismutases and Manganese: An Efficient Protection Against Oxidative Stress*

SODs are metal-containing oxidoreductases that catalyze the dismutation of superoxide—oxidation to dioxygen and reduction to hydrogen peroxide (see Fig. 7.3). They maintain the concentration of superoxide inside cells at very low levels (less than 50 pM in *E. coli* or mammalian cells) [14, 15, 27]. They are crucial proteins in the protective antioxidant arsenal, since superoxide is the first step in the ROS cascade from dioxygen to water (see Fig. 7.1). Mammalian cells produce three different SODs, involving either copper-zinc or manganese metal centers: SOD1, CuZnSOD found in the cytosol, in the nuclear compartments, and in the mitochondrial intermembrane space; SOD2, a MnSOD found in the mitochondrial matrix, which is its exclusive location in human beings; and SOD3 (EC-SOD), an extracellular CuZnSOD, found in extracellular matrix of tissues and extracellular fluids (such as plasma) [1, 9]. SODs are compartmentalized, which means they are not able to cross membranes, move from one organelle to another, nor enter/leave cells. The mitochondrial MnSOD has a particular biological importance in mammals: its knockout is lethal to newborn mice [28, 29], whereas this is not the case for CuZnSOD [30].

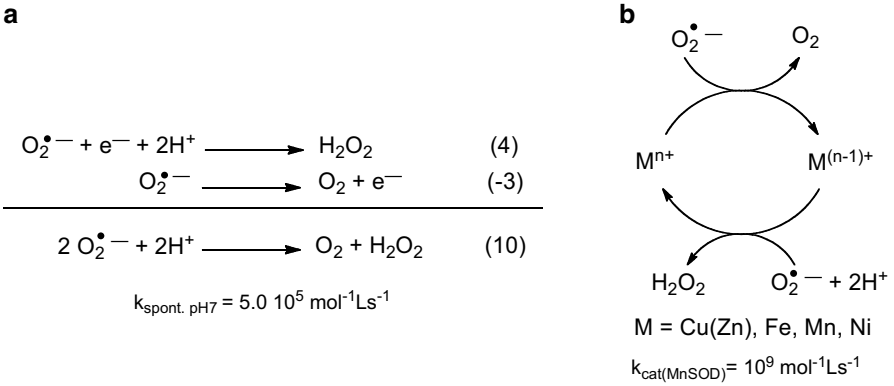

Fig. 7.3 (**a**) Spontaneous superoxide dismutation—or autodismutation, and (**b**) simplified ping-pong mechanism for the catalysis of superoxide dismutation. The kinetic data are from [61] and [58]

In addition, dysregulation of MnSOD or MnSOD natural mutations—an example of protein polymorphism—has been proposed to be involved in cancer [20]. Other metal ions can also be found as cofactors in non-mammalian SODs: iron in FeSOD, which coevolved with MnSOD from a common ancestor, shows high degrees of both sequence identity and structural homology with MnSOD and was discovered in 1973 [31]; and nickel in NiSOD, which belongs to a rarer SOD family discovered in 1996 [32].

SODs have been found in almost all aerobic, facultative anaerobic, and even in some anaerobic organisms, where they have been sought. An exception is the case of microaerophilic and anaerobic bacteria that contain a superoxide reductase (SOR), which detoxifies superoxide by its reduction into H_2O_2. Detoxification of superoxide by SORs avoids O_2 release which would be expected to be toxic in air-sensitive microorganisms [9, 33]. When SOD are not present or show a low activity (e.g., *Leptospira interrogans* serovars [34], *Lactobacillus plantarum* [35], and *Neisseria gonorrhea* [36]), cells are either very rich in catalase or show a high intracellular concentration of Mn^{II} (up to 15–30 mM in *Lactobacillus plantarum* [35]). These observations are interesting in several ways:

(a) Few organisms are found without any SOD or SOR: this observation emphasizes the importance of superoxide removal and the need for protection against superoxide.
(b) Viable organisms, although rare, are found with no SOD but with high concentration of catalase, which seems to rescue them in the absence of SOD or SOR. This could suggest that the key feature is to limit the time of co-residence of superoxide with hydrogen peroxide. $O_2^{\bullet-}$ and H_2O_2 are inevitably found at the same location in biological systems because superoxide self-dismutation produces H_2O_2. This leads potentially to Haber–Weiss chemistry (see Fig. 7.2) in the presence of soluble iron(II) or copper(I), redox states that can be found in cells where the environment is reducing [37]. Limiting the co-residence time of H_2O_2 and $O_2^{\bullet-}$ restricts possible Fenton/Haber–Weiss chemistry that would lead to the continuous production of the deleterious $HO^{\bullet}$ by the use of superoxide for Fe or Cu redox cycling.
(c) Organisms such as *Lactobacillus plantarum* suggest that, beside SOD/SOR protection, high concentration of manganese is another possible rescue mechanism from ROS damage.

The question of the speciation of Mn ions in cells and of the involvement of non-proteinaceous Mn-complexes in antioxidant defense has recently been a matter of intense research [18, 38]. Due to its high redox potential (1.51 V vs. NHE, see Figs. 7.4 and 7.12), the hexaaqua Mn^{III}/Mn^{II} couple is not an efficient catalyst for superoxide dismutation, which would require a redox potential in between the redox potentials of the two couples related to both superoxide oxidation and reduction (see Fig. 7.4) [39, 40]. But the hexaaqua Mn^{III}/Mn^{II} couple can act as a stoichiometric scavenger. In addition, the presence of intracellular coordinating anions, such as lactate or phosphate, has been shown to lead to complexes with an effective SOD activity, associated with cellular oxidative stress resistance [35, 39, 41, 42]. Even if

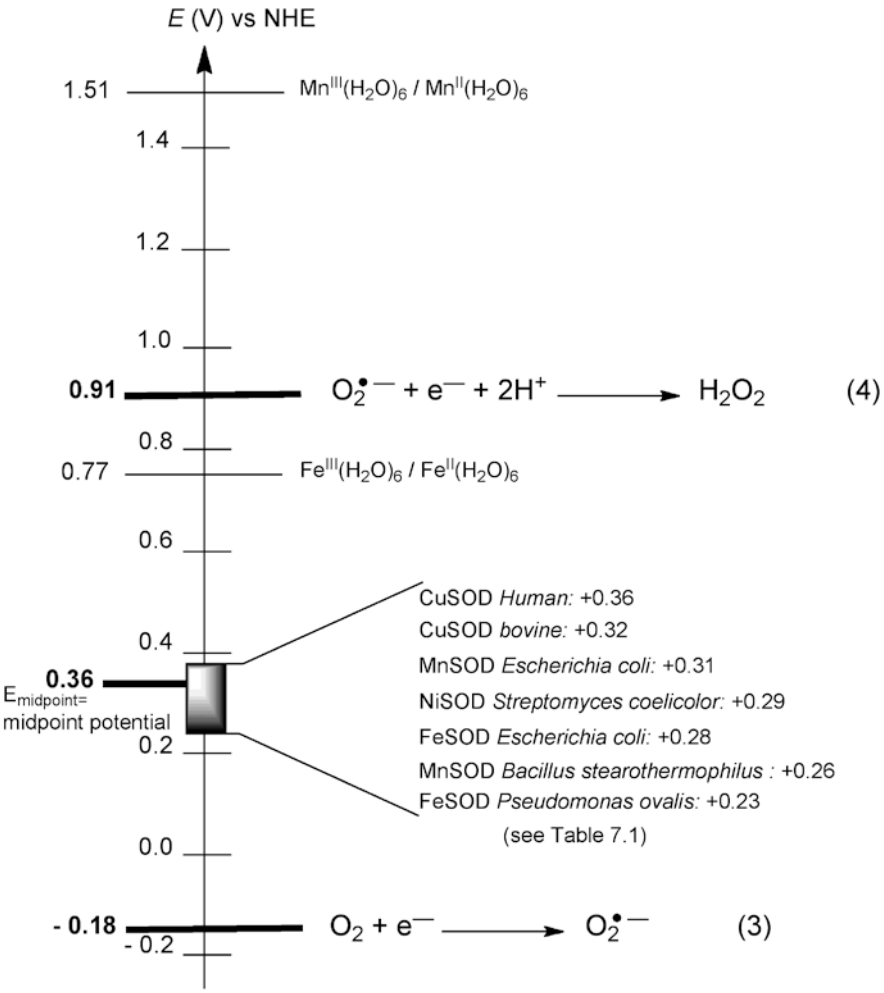

Fig. 7.4 Standard redox potentials E°′ V vs. NHE for superoxide at pH 7 [7], midpoint potential optimal for catalysis of the dismutation ($E_{midpoint}$) [60], redox potentials reported for several SOD (see also Table 7.1) and for hexa-aqua Mn^{III}/Mn^{II} and hexa-aqua Fe^{III}/Fe^{II}

their rate of superoxide dismutation is lower than that of SODs, the corresponding Mn complexes can efficiently protect cells if sufficiently concentrated. Mn ion can exchange its ligands, especially at the +2 oxidation state, and biological environments abound with coordinating molecules. It is thus possible that Mn complexes formed inside cells could act as efficient SOD mimics: they are possibly in dynamic exchange, and hence difficult to isolate and characterize, but some may show redox potential appropriate for SOD activity. Recently, it has been shown that this battery of Mn antioxidants was tightly regulated by specific pathways in *Saccharomyces cerevisiae* [43], indicating these non-proteinaceous Mn-antioxidants are not only passively formed in cells [18].

7.2.3 SOD Discovery: A History of Anti-Inflammatory Properties (See Also Chap. 1)

Through their anti-superoxide activity, SODs show interesting pharmacological properties. Indeed, the antioxidant and anti-inflammatory properties of SODs are closely associated with their discovery, which occurred, not once but three times [22]. In 1938, Mann and Keiling, interested in the speciation of copper ion in blood, isolated from horse serum a protein described as a copper-binding protein that they called hemocuprein [44]. Twenty years later, a similar copper-protein, erythrocuprein, was isolated from human erythrocytes [45]. In both occasions, several enzymatic activities for these proteins were sought: catalase, peroxidase, cytochrome oxidase, or carbonic anhydrase activities, by Mann and Keimann [44] and oxidase activities with various substrates by Markowitz et al. [45]. But none could be found.

In 1931–1932, Pauling had suggested that superoxide, as a possible "*intermediate between molecular oxygen and hydrogen peroxide, should have enough stability to exist*" [46] and superoxide had been characterized as potassium superoxide by Nauman in 1934 [46–48]. However, the idea that superoxide could be involved in biological environments appeared only in 1968, when Knowles found that superoxide could be produced by xanthine oxidase [49, 50]. Taking advantage of this finding, McCord and Fridovich showed that erythrocuprein has an enzymatic activity associated with the dismutation of superoxide and they designed an assay that is still widely used today (see insert at the end of Chap. 7) [51]. Independently, Huber et al. isolated a protein from bovine liver, orgotein, based on its anti-inflammatory properties. The physicochemical properties of this protein are close to those of hemocupreins and erythrocupreins [52]. The link between inflammation and superoxide was suggested soon after by Babior et al. [53]. Indeed, inflammation is a physiopathological condition characterized by a high production of ROS by macrophages or immune cells. This chemical signal causes the recruitment of additional ROS-producing cells and enhances the biological response with a higher flow in ROS meant to kill pathogens but leading also to unintended biological damage.

7.2.4 Mimicking SODs by Low-Molecular-Weight Complexes: SOD Mimics

Since this pioneering work, purified SODs have been successfully used in clinical trials [26, 54], and antioxidants in general, including SODs, are now quite well documented for their beneficial effects in oxidative stress situations [22, 24–26]. Nonetheless, major drawbacks limit the applications of the SOD enzymes in therapeutics: cost of production, immunogenicity, short half-life in plasma, inefficient per os delivery added to limited cellular accessibility [24], and clearly, stabilizing SODs in biological environment is not straightforward [55]. These limitations can

be overcome by using low-molecular-weight complexes reproducing the *catalytic activity* of SODs, also called SOD mimics [17, 56]. In the literature, SOD mimics have been designed to react with superoxide outside of any cellular context [17, 56] and some are reportedly efficient in ameliorating oxidative stress, both in cells and in vivo [24–26, 54, 57]. Of note, we have used here a circumlocution to designate studies performed outside any cellular context, e.g., in UV-vis cuvette as in the McCord and Fridovich assay: in vitro, a term frequently used by chemists, is not fully appropriate here as for cell biologists it refers to studies in cell cultures as in contrast with studies performed in animal models. To avoid any misunderstanding, we refer herein to activities evaluated outside any cellular context as *intrinsic activities* in contrast with *in cell activities* and in vivo *activities*. In the case of SOD mimics, intrinsic activity will refer to the kinetics of the reaction with superoxide (see insert for methods of evaluation), possibly the catalytic constant in case of a true catalytic SOD mimic.

To obtain a complex acting as an SOD mimic with therapeutic efficacy against oxidative stress, a primary need is to design nontoxic complexes with a good intrinsic activity. Some excellent reviews have been previously published on the rational design of SOD mimics to delineate important features for an efficient intrinsic activity [17, 56], or for application in therapeutics [23–26, 54, 57]. In the following sections, we will focus on approaches aimed at designing SOD mimics bioinspired by SODs' main features, and more particularly those of MnSODs. We will draw the main characteristics of SODs on which chemists focused for the design of SOD mimics. We will then describe different strategies set up to enhance the activity of SOD mimics following the footsteps of Nature.

7.3 SODs Physicochemical Characteristics: A Guideline for Chemists

All SODs, whatever the metal ion involved at the active site, are very efficient enzymes, reacting with superoxide with kinetics close to the diffusion limit [58], and the parameters responsible for this efficient activity have been carefully analyzed (for an excellent recent review, see Sheng et al. [1]). As already mentioned, SODs can be classified into three subfamilies of different lineages: (a) CuSOD, with their bimetallic $Cu^{I/II}$-Zn^{II} active site, (b) Fe or MnSOD, with $Fe^{III/II}$ or $Mn^{III/II}$ active site, which are evolutionary related and share high degrees of sequence identity and structural homology, and (c) NiSOD, a rarer family of SOD with a $Ni^{III/II}$ active site. Interestingly, these families share some common features delineated below, a signature of a convergent evolution and indicating the strong efficiency of these particular characteristics and mechanisms selected by Nature [1]: (a) tuned redox potential (b) electrostatic guidance of the anionic superoxide, and (c) compartmentalization into specific organelles.

7.3.1 Redox Potential: The Main Determinant for Catalytic Activity

Redox Tuning at the Active Site of SODs

The superoxide anion is metastable and the reaction of dismutation is indicated in Fig. 7.3. The catalysis of this reaction is a redox process, involving both Mn^{II} and Mn^{III} oxidation states in the case of MnSOD, to respectively reduce superoxide into H_2O_2 in the presence of protons and to oxidize it into O_2. To be thermodynamically competent to carry out both steps, the redox potential of the Mn^{III}/Mn^{II} couple must lie between those of the two couples involving the superoxide anion, $O_2^{\bullet-}/H_2O_2$ and $O_2/O_2^{\bullet-}$, as indicated in Fig. 7.4, at pH 7 and with a concentration of dioxygen of 1.23 mM, which is that in water under standard conditions, 25 °C and 100 kPa [7]. In addition, for optimal kinetics, one should consider the fact that the closer the redox potential of two couples, the faster the reaction between them [59, 60]. Therefore, the value of the Mn^{III}/Mn^{II} redox potential optimizing the kinetics of the overall catalytic cycle is the mid-potential, at about 0.36 V vs. NHE (see Fig. 7.4) [60]. As a consequence of this redox tuning, the two half-reactions ((4) and (−3), see Figs. 7.1 and 7.3) proceed at the same rate, which is the overall optimal rate for the catalytic cycle.

Interestingly, all SODs indeed meet this criterion with the redox potential of Cu^{II}/Cu^{I}, Mn^{III}/Mn^{II}, Fe^{III}/Fe^{II}, and Ni^{III}/Ni^{II} falling within a very narrow range around 0.2–0.4 V vs. NHE (see Fig. 7.4 and Table 7.1). This observation is very informative as it clearly shows that the redox potential is a key parameter to be tuned for an efficient SOD activity. It should be further emphasized that this narrow potential range is very striking, since the intrinsic redox characteristics of the aqueous metal couples $M^{(n+1)}{}_{aq}/M^{n+}{}_{aq}$ involved in SODs are quite different. To take the example of Fe and MnSODs that has been extensively studied by Miller et al. [1, 65], the redox

Table 7.1 SODs redox potentials (see also Fig. 7.4)

SOD	Organism	pH	E_m (V vs. NHE)	References
CuSOD	Human	7.4	0.36	[62]
CuSOD	Bovine	7.4	0.32	[62]
MnSOD	*Escherichia coli*	7	0.31	[63]
MnSOD	*Escherichia coli*	9	0.18	[63]
NiSOD	*Streptomyces coelicolor*		0.29	[64]
FeSOD	*Escherichia coli*	7	0.28	[60]
FeSOD	*Escherichia coli*	9	0.12	[60]
MnSOD	*Bacillus stearothermophilus*	7	0.26	[63]
MnSOD	*Bacillus stearothermophilus*	9	0.12	[63]
FeSOD	*Pseudomonas ovalis*	7	0.23	[60]
FeSOD	*Pseudomonas ovalis*	9	0.19	[60]

Note that the E°s of SODs can be difficult to measure precisely due to slow equilibration and other slightly different values can be found in the literature

potential of the hexaaqua complexes of $Mn^{III}_{aq}/Mn^{II}_{aq}$ in aqueous environment is 1.51 V vs. NHE and that of $Fe^{III}_{aq}/Fe^{II}_{aq}$ is 0.77 V vs. NHE (see Fig. 7.4). The role of the apoprotein is then to tightly control the metallic redox potential. The question of the tuning of redox potentials at the active site of redox proteins in general, including Fe/MnSOD and also copper proteins, has evoked some interest lately [1, 65–67]. Several parameters can be modulated for this tuning, including the nature of the coordinated Lewis bases, their protonation state, and the geometry of the coordination sphere. Tuning can occur in proteins, but also in low-molecular-weight complexes [40, 68, 69]. This is discussed in more detail below (see next section).

This redox tuning is key to the catalysis and the catalytic nature is most valuable for the design of a drug candidate. A catalytic drug is a compound displaying therapeutic properties based on catalysis [70]. To date, the conventional approaches to drug design consist of seeking for small organic or inorganic molecules that bind to the active sites of proteins and are thus stoichiometric reagents. SOD mimics belong to another class of therapeutic agents displaying a catalytic activity by performing both reduction of superoxide into H_2O_2 and its oxidation into O_2 (see Fig. 7.3). Catalytic complexes have been labeled *true SOD mimics*, in contrast to stoichiometric scavengers such as nitroxides [23]. Catalysis has many advantages, including the opportunity to lower dosage, which is important in a therapeutic perspective. The superoxide steady-state concentration is low in biological systems: 20–40 pM in aerobic log phase wild type (WT) *E. coli* (hence containing endogenous SOD) and 300 pM in SOD-deficient *E. coli* mutant [14]. As superoxide is continuously produced, an efficient control of its flow requires either an efficient catalyst or a stoichiometric scavenger in large amounts and/or of continuous renewal. In the case of a redox process in biological media, apparent catalysis is achievable through redox cycling using cell reductants, as in the superoxide reductase enzymes (SOR): these Fe^{II}-native-state enzymes are oxidized to Fe^{III} by superoxide and reduced back to their active Fe^{II} state by endogenous reductants rather than by superoxide itself [71, 72]. It should be kept in mind that it is not always easy to distinguish between highly concentrated scavengers and true catalytic species in assays used to characterize anti-superoxide activity: a true catalytic SOD mimic is able to perform several turnovers and is efficient even in a large excess of superoxide [73] (see insert at the end of Chap. 7).

Tuning of the Redox Potential of a Redox Metal Couple: What Tricks?

The redox potentials of $M^{(n+1)+}/M^{n+}$ can be tuned by exploiting the coordination sphere of the metal ion. This can be achieved in redox metalloproteins by the environment offered by the apoproteins, and can be translated at the level of low-molecular-weight complexes through the selection of ligands and second coordination sphere (see Sect. 7.4.2).

The redox potential can be controlled by the nature of the coordinated Lewis bases through electronic effects. For instance, increasing the number of the S or O-donors with regard to the N-donors will lower the potential by increasing the electron density onto the metal center. This can be easily achieved in proteins, by

playing with coordinating amino acid side chains that can be N-donors as in histidine or histidinate, O-donors as in aspartate, glutamate, or tyrosinate, and S-donors as in cysteine, cysteinate, or methionine. Note that amidate from the terminal position or in the proteic chain are rarer, but can also be involved in metal coordination.

The protonation state of the coordinated ligand (water/hydroxide, histidine/histidinate, etc.) can be easily modulated in proteins within a network of hydrogen bonds. The more negative the ligand, the more easily the high oxidation and positive redox metallic states will be obtained and the lower the reduction potential. As an example, the redox potential of MnSOD or FeSOD was found to depend on the pH with a decrease in redox potential when pH is increased (see Table 7.1). This was rationalized by a deprotonation of the coordinated water [60], the higher oxidation state being more stabilized by the hydroxide OH^- ligand than by H_2O. It has been clearly demonstrated that the coordinated water molecule can switch from H_2O to OH^- depending on the oxidation state of the metal ion. This is associated with a process whereby proton and electron transfer are coupled (proton-coupled electron transfer, PCET), with a tight control of an H-bond network extending to the second coordination sphere [65]. The effect of protonation-deprotonation of coordinated imidazoles was also studied in low-molecular-weight complexes, in iron porphyrins with an axial imidazole [74] or nonporphyrinic complexes [75–78] with a ΔE of about—300 mV per lost proton, which is similar to protein systems [65]. In another study, PCET was observed in a low-molecular-weight Mn-complex, with coordinated water deprotonation occurring upon oxidation of Mn^{II} to Mn^{III} [79].

The geometry imposed upon the metal ion is also another possible source of redox-control, as geometric constraints may induce entatic states [80] and stabilize unusual redox states. Imposing a geometric environment on a metal cation can be achieved by selection of ligands/apoproteins in a constrained fashion motif or embedded in a rigid matrix, which organizes the resulting coordination sphere as in a template [69]. As described in any inorganic chemistry textbook, a specific redox state and d^n configuration of a metal ion is usually associated with a particular geometry. Interestingly, such relationship can be reversed: indeed, if a ligand imposes a specific geometry on a metal cation, this can, in turn, control the reduction potential of the redox couples related to the cation. Let us take the example of the Mn^{III}/Mn^{II} redox couple, of interest here. Hexaaqua Mn^{II} is rather stable and the Mn^{III}/Mn^{II} reduction potential of fully dissociated Mn salts in water is 1.51 V vs. NHE, consistent with a stable Mn^{II} state in aqueous environment. Water molecules as ligands organize themselves around the "free" Mn^{II} ion in an octahedral environment. Mn^{II} coordinated by flexible organic ligands will display a similar behavior, with a redox potential controlled by the electrodonating properties of the coordinated Lewis bases. But, in the case of a ligand imposing a specific geometry, there can be an effect of the constrained geometry on the redox potential. This can be understood as *geometric control of the redox potential* and was described in the case of Cu^{II}/Cu^{I} constrained complexes [69] but can also apply to Mn^{III}/Mn^{II} complexes [40, 68]. Mn^{III}, as a d^4 ion with an e (e_g) singly filled orbital, will prefer a geometry with an axial distortion from the octahedral structure, to lift the degeneracy of the e

orbitals which is a stabilizing process known as the Jahn–Teller distortion [81, 82]. In contrast, Mn^{II}, as a d^5 ($S=5/2$) with half-filled t_2-e set (t_{2g}-e_g), shows no ligand-field stabilization energy (LFSE) and hence no geometric preference. Finally, a ligand imposing an axial distortion will stabilize the Mn^{III} state over the Mn^{II} state [40, 68], and this corresponds to a decrease in redox potential.

7.3.2 *Electrostatic Guidance*

Superoxide dismutases react with superoxide at a rate close to the diffusion limit. This efficiency is most surprising considering that the metal active site represents a surface that is less than 1 % of the enzyme [83–85], and that the net charge of SOD, which shows an isoelectric point (pI) ranging from 4.6 to 6.8 depending on the lineage, is negative at physiological pH [84, 85]. Calculations of electrostatic potential in CuSOD [83, 85] have led to the idea of an electrostatic guidance of the negatively charged superoxide by a cluster of positively charged amino acids within the substrate entrance channel [85], with an invariant arginine and the charge-stable Zn^{2+} ion in close proximity to the redox active Cu^{II}/Cu^{I} metal ion. A decrease in the k_{cat} was observed when ionic strength was increased for MnSOD, FeSOD [84, 86], and CuSOD [87, 88] in agreement with an electrostatic favorable interaction between the protein and its substrate, indicative of a positively charged target for the superoxide on the protein. Acylation of lysines eliminates this salt effect [84], and a network of positively charged amino acids, namely histidines, has been identified in X-ray structures [89] and by Brownian dynamics [86]. In some sense, we can consider that there is a double topographic effect, with the negatively charged protein surface repelling the superoxide and directing it towards the positively charged funnel, which then drives it to the active site (see Fig. 7.5). The electrostatic positively charged loops in the SOD proteins are thus important for long-range guidance from the protein exterior towards the active site, and attraction of superoxide by positive charges is a more general mechanism that can also be effective in low-molecular-weight molecules, as it will be described below (see Sect. 7.4.3).

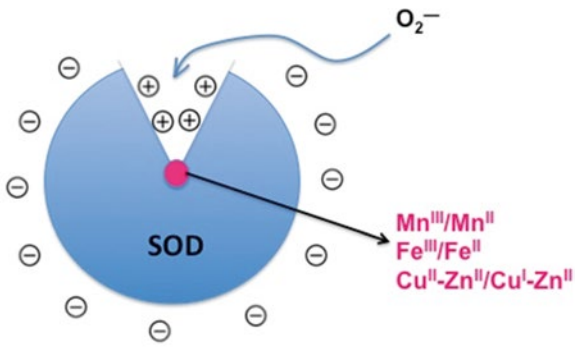

Fig. 7.5 Schematic representation of the electrostatic guidance: superoxide is repelled from the negatively charged surface towards the positively charge funnel leading to the active site

7.3.3 *Compartmentalization*

Another important feature of SODs is that they are compartmentalized: due to their size and negative net charge at physiological pH (see pI above), they are unable to cross cell membranes. MnSOD is synthesized in the cytosol, and imported into the mitochondria through an appropriate 24-amino acid targeting sequence which is then cleaved [90]. As mentioned above, mitochondrial MnSODs are key proteins in the protection of mammalian cells from oxidative stress and, indeed, MnSOD knockout is lethal to newborn mice [28, 29], whereas murine CuSOD is not crucial to survival [30]. Mitochondrial MnSOD expression is known to be altered in a wide range of diseases [20]. Mitochondria are the main cellular location at which superoxide is produced through uncoupling of the respiratory complexes involved in the reduction of dioxygen to water. The uncontrolled production of superoxide, associated with other ROS and RNS (reactive nitrogen species), induces oxidative damage leading to mitochondria dysfunction and contributes to several physiopathological processes (see a quick list in Sect. 7.2.1) or to cell death [20, 22, 24–26]. Targeting this organelle thus appears to be a key parameter to consider in the design of efficient anti-superoxide agents [24, 91–94].

The mitochondrion or the mitochondrial network is a dynamic structure with many shapes, which can take a form ranging from numerous individual capsules, most often depicted in textbooks, to a single large interconnected tubular network, as a net cast over the cell. They are key organelles: powerhouse of the cell, center of respiration and ATP production, and essential in lipid metabolism [95]. Their interior is protected by a double membrane, with a large membrane potential of up to 180 mV, negative in the interior. Smith and Murphy have set up a strategy to target small molecules to the mitochondria, taking advantage of this large membrane potential: lipophilic positively charged cations, such as triphenylphosphonium moieties [93], can be appended to various molecules in order to encourage the targeting of the mitochondria. Other groups have developed oligoguanidinium derivatives, showing a hydrophobic positively charged character as vectors to the mitochondria [96]. Cellular membranes contain negatively charged phospholipids, with polar and negatively charged groups pointing outward from the membrane and lipophilic chains inward. To cross them, a molecule must be neutral or positively charged, and must also be amphiphilic to pass through the polar layer and the hydrophobic membrane interior. The delocalized positive charge of the triphenylphosphonium or oligoguanidinium moieties enables easy crossing and induces an accumulation at the mitochondria. This was applied in the field of SOD mimic design as described in Sect. 7.4.4.

7.4 Mimicking SOD: A Challenge for Chemists

Various strategies have been developed to design efficient metal-based anti-superoxide agents [17, 26, 40, 54, 56]. As seen above, the common physicochemical characteristics shared by SODs from different lineages [1], namely, tuned redox

potential, electrostatic attraction of superoxide, and mitochondria localization for MnSOD, constitute a guideline for the development of bioinspired SOD mimics. The main challenge for chemists in the field is the design of nontoxic stable complexes, with tuned redox potential and charge that would react quickly with superoxide, and show good cellular availability and possibly accumulation at the mitochondria. Of note, among the four metal ions responsible for the redox process at the active site of SODs (Cu, Fe, Mn, and Ni), manganese is most probably the least toxic [9, 16, 17], in particular in an oxidative stress context that could activate Haber–Weiss chemistry for copper and iron. This is why, although some neurotoxicity has been described [23], Mn ion is now the leading metal ion in the field of SOD mimic design for therapeutic use.

The stability and inertness of complexes are important parameters to keep in mind when designing metal-based drugs, as biological environments are rich in metal-coordinating molecules. Mn^{II} can be in fast exchange when coordinated to monodentate ligands, whereas more inert structures are obtained with Mn^{III}. The question of the speciation of manganese complexes in biological environments (see Sect. 7.2.2) is crucial to their bioactivity. Endogenous biologically available ligands have been shown to potentiate the antioxidant activity of Mn ions, most likely by modification of the Mn^{III}/Mn^{II} redox potential. This is the case with anions such as lactate or phosphate [35, 39, 41, 42]. Other ligands, such as citrate or EDTA, are thought to inhibit the activity [39, 40]. As Mn^{II} is a d^5 ion, the ligand field induces no stabilization and thus the thermodynamic constants for the association of Mn^{II} with most ligands are in a low range. Therefore, the requirement in association constants to avoid exchange with endogenous Lewis bases is less drastic for Mn^{II} than for other metal ions such as copper or iron. Polydentate ligands [40, 97, 98], particularly with a cyclic structure as in Mn^{II} cyclic polyamines (M40403) [25, 26, 57, 99] or porphyrins, stable at the Mn^{III} state [23], have been described to display association constants higher than 10^6 (or dissociation constants smaller than 10^{-6}), which should be enough considering that the archetypal bioligand, human serum albumin (HSA), display an association constant for Mn^{II} of about 8.4×10^3 (or 1.2×10^{-4} for the dissociation) [100].

The next criterion, after stability and inertness, is the kinetics of the reaction with superoxide. As stressed by Batinić-Haberle et al. [23], to be therapeutically active, a compound must be kinetically competent, which means it should react with superoxide with a kinetic constant higher than the autodismutation (see Fig. 7.3a) but, even more valuable, be a catalyst of its dismutation and, the faster, the better. There is a positive correlation between the catalytic kinetic constant for the superoxide dismutation, or $\log(k_{cat})$, and the therapeutic effects [23]. But other parameters are also of importance for in vivo efficacy. As shown in a study by Valentine et al., some derivatives can display a high intrinsic activity and be inactive in cellular models [101]. These authors assayed the ability of an assortment of SOD mimics to rescue *Escherichia coli* and *Saccharomyces cerevisiae* mutants lacking SOD. Only one of the compounds, a positively charged Mn^{III} porphyrin known to accumulate in the mitochondria [102], was found to be active in cells. The authors suggested that the absence of activity of the other derivatives was due to mislocation. In contrast, the

active Mn^{III} porphyrin was able to reach the mitochondria, which is the appropriate location for an optimal rescue of these SOD-lacking strains. To be actually bioactive, a SOD mimic must reach its target, which can be the extracellular space, the cytosol or various organelles depending on the physiopathological conditions and origin of the oxidative stress. More generally speaking, the bioactivity of any kind of derivatives is in some sense the combination of its intrinsic activity, related to the redox potential in the case of SOD mimics, with the bioavailability and the cellular location [23, 103].

In the following section, we will describe (a) design of complexes directly inspired by the SOD active site; (b) strategies developed by chemists to tune redox potential to the $E_{midpoint}$ optimal value of 0.36 V vs. NHE, as one of the key parameters; (c) strategies developed by chemists to mimic efficient electrostatic attraction; and (d) strategies to enhance the bioavailability and control location within the cell. Structures discussed in this chapter are depicted in Figs. 7.8 and 7.11a, b.

7.4.1 Complexes Directly Inspired by SOD-Active Site (Mn-$N_{3/4}O$ Complexes)

Policar et al. have designed a series of low-molecular-weight manganese complexes based on a tertiary amine or 1,2-diamino-ethane, directly inspired by the active site of SOD [40, 73, 97, 104–108], to reproduce the chemical environment of the Mn ion in SOD (see Figs. 7.6 and 7.8), with the initial goal of characterizing intermediates in the catalytic cycle of MnSOD. In native SOD, Mn^{III} is in a trigonal bipyramidal (TBP) geometry with an N_3O/water coordination core with one monodentate aspartate and two histidine moieties in the median triangle/equatorial plane (in green in Fig. 7.6), and a farther histidine with a water molecule (H_2O or HO^-) in the two apical positions.

The particular axial TBP geometry at the active site of SOD is important since it geometrically favors Mn^{III} over Mn^{II} and thus contributes to the tuning of the redox potential (see above) [40, 68], which must be lowered from 1.51 V vs. NHE down to *ca.* 0.36 V vs. NHE. In addition, the coordination number (CN) is lower than six, which is favorable for the direct coordination of the superoxide ion to the metal center. Indeed, superoxide is thought to coordinate to the active site of SOD as shown by experiments with the isostere and isoelectronic analog azide N_3^- [1, 110, 111]. Of note, superoxide can act either as an L-ligand or as an X-ligand leading to a non-redox coordination (L-ligand) or to an oxidative addition (X-ligand) onto the metal ion (see Fig. 7.7). Low CN complexes are difficult to prepare with low-molecular-weight ligands. In proteins, the polypeptide chain plays the role of a bulky matrix able to sterically impose low denticities. But with flexible open ligands, high-denticity structures are frequently obtained, with the coordination of a solvent molecule or Lewis bases acting as bidentate ligands possibly bridging two metal ions from two different molecular units. The corresponding complexes are sometimes said to be *coordinatively saturated*. Superoxide coordination will lead to the displacement of a ligand or

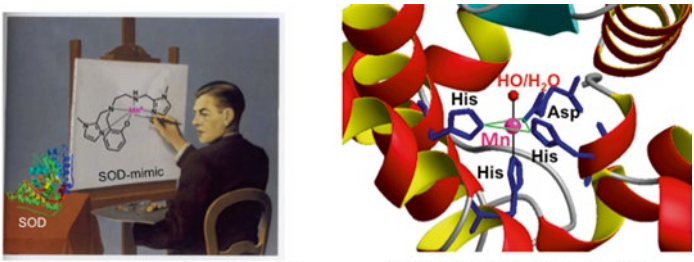

Fig. 7.6 Allegory of bioinspired chemistry: mimicking SOD from Nature—Active site of SOD, structure from [109]

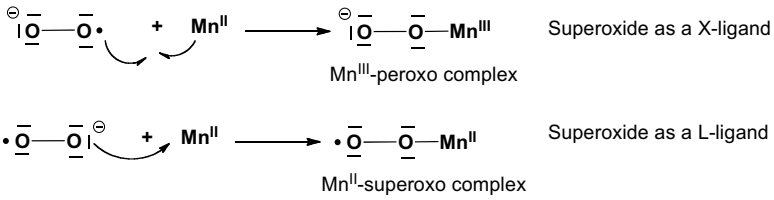

Fig. 7.7 Superoxide as a L or X ligand

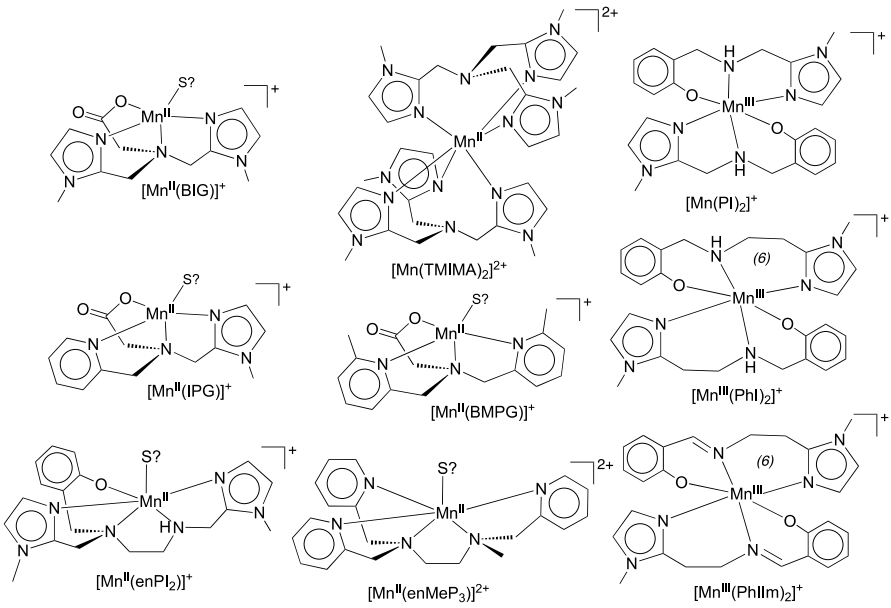

Fig. 7.8 Structure of the complexes discussed in Sect. 7.4.1: mononuclear units obtained after dissolution (see *text*). *S*? corresponds to possible solvent molecule. See: [40, 73, 97, 104–108]. *(6)* indicates a 6-membered metallacycle whereas all the others are 5-membered rings

to even higher coordination number, achievable if there is not too much steric crowding.

Starting from complexes with Mn^{II} coordinated by a tripodal amine functionalized with two imidazole and one carboxylato moieties, Policar et al. introduced modifications (see Fig. 7.8) to increase bulkiness around the metal ion (picolyl moieties in BMPG, hexacoordination in $[Mn(TMIMA)_2]^{2+}$) or to tune the redox potential of the Mn^{III}/Mn^{II} couple to the $E_{midpoint}$ encountered in SODs (coordinated Lewis bases such as imidazole, carboxylate, or phenolato). In the course of this research, they isolated original 1D coordination polymers with Mn^{II}-OCO-Mn^{II} along the polymeric chain, with bridging carboxylatos in an unusual *syn-anti* coordination mode [104]; dimeric structures with a bis-μ-carboxylato bridge [97] or a bis-μ-phenolato bridge [105]. Some other complexes were isolated in the solid state as monomers with two tridentate ligands [40, 106]. Although the ligands in the series all offer a denticity lower than six (tetradentate N_3O or pentadentate N_4O), the structures observed in the solid state are all hexacoordinated, with carboxylato or phenolato shared between two metal ions or coordinated exogenous Lewis bases, most generally the crystallization solvent (methanol, water). This series thus illustrates this propensity to acquire a coordinatively saturated coordination sphere in the case of low-molecular-weight ligands. In aqueous solution, the bridges are disrupted, leading to monomeric Mn^{II} complexes, as shown by electron paramagnetic resonance—characteristic 6-line signal for the Mn^{II} $I=5/2$ $S=5/2$ complexes [40, 97, 105]. Most probably, the coordination sphere is saturated with solvent molecule(s) (S in Fig. 7.8). It should be noted that a wave in cyclic voltammetry is not always easy to record with this kind of Mn^{III}/Mn^{II} complex [40, 112, 113], probably due to slow electron exchange. The use of collidine, lutidine, or PIPES buffers may be efficient to reveal the wave, which may not be fully reversible [40, 112]. All the redox potentials of the complexes in the series presented in Fig. 7.8 are in the range expected for the catalysis of superoxide dismutation (see Fig. 7.4). From these studies, it appears that a phenolato ligand is more efficient to stabilize Mn^{III} than a carboxylato ligand and seems thus to be a better electronic analog for the monodentate carboxylato in SOD. The optimal ligand in the series is $enPI_2$, which offers higher pentadenticity with a higher association constant for the Mn complex [168] and a Mn^{III}/Mn^{II} redox potential very close to that of SOD [105].

The reactivity with superoxide was studied in both anhydrous aprotic medium and aqueous solution.

In Anhydrous Aprotic Medium [40, 97, 107, 114]

Superoxide can be introduced as KO_2 in the solid form [107], in solution (dimethylsulfoxide DMSO, acetonitrile ACN) [40, 97], or produced electrochemically by reduction of dissolved O_2 [97, 114]. In anhydrous aprotic medium, where no protons are available for the reduction of superoxide into hydrogen peroxide (see Fig. 7.3), H_2O_2 cannot be released and intermediate adducts with the Mn complexes can be isolated: by reacting KO_2 in DMSO or ACN with Mn^{II}-complexes, MnOO

adducts were characterized by low-temperature spectroscopies, including UV-visible spectroscopy and electron paramagnetic resonance (EPR). These adducts displayed a very nice blue color (see Fig. 7.9). For the first time, using parallel mode EPR, an Mn^{III} redox state ($S=2$) was unambiguously characterized, within a Mn-coordinated peroxo species [107]. Clearly, the reaction of Mn^{II} with superoxide in these complexes can be rationalized as an oxidative addition onto the Mn^{II} ion with superoxide being an X-ligand (see Fig. 7.7).

Similar Mn^{III}-peroxo adducts are expected when reacting Mn^{III} with H_2O_2, which is redox-equivalent to $Mn^{II}+O_2^{-}$. Other research groups have also characterized similar MnOO intermediates by reacting H_2O_2 with Mn^{II} at low temperature, which is clearly not redox-equivalent to $Mn^{II}+O_2^{\bullet-}$ or $Mn^{III}+H_2O_2$, but there is always an excess in H_2O_2 [115–119] and most probably the first step is a slow oxidation into Mn^{III}, which then reacts with H_2O_2. This kind of adduct can be labeled $\{MnOO\}^6$ [73] by analogy with the Enemark-Feltham nomenclature for Fe-nitrosyl [120]. These evolve at ambient temperature leading to Mn^{III}-Mn^{IV} di-μ-oxo derivatives

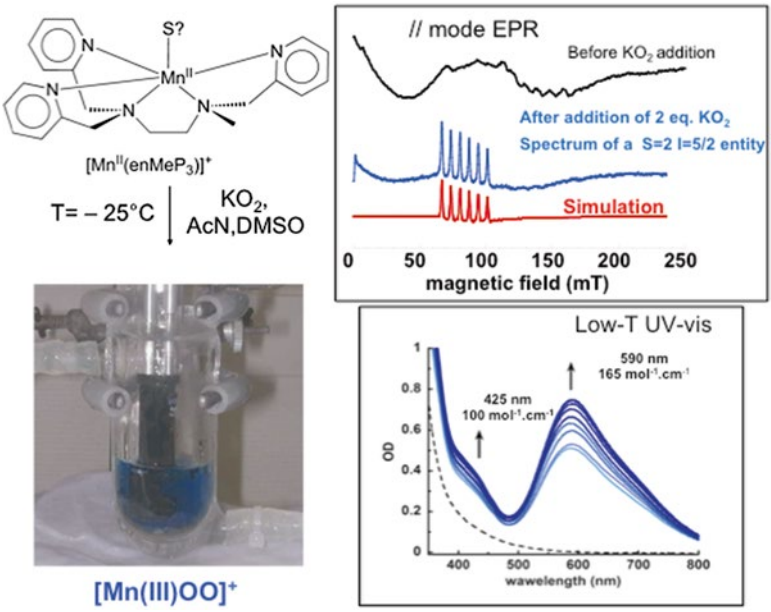

Fig. 7.9 Reaction in anhydrous medium of KO_2 with a Mn^{II}-tris-pyridyl-bis-amino complex. On the *left*: Photography showing the blue color of the Mn-OO adduct at −25 °C. Set-up to record low-temperature UV-vis spectra, with an immersion UV-vis probe (in *black*) within a double-jacket low-temperature cell. On the *right, top*: parallel mode EPR spectra showing that a Mn^{III} species was obtained. Recording conditions: microwave power 2 mW; modulation amplitude 5 G; modulation frequency 100 kHz; time constant 40.96 ms; $T=5$ K; parallel mode: $\upsilon=9.417$ GHz. On the *right, bottom*: UV-vis spectra recorded using the immersion probe (photo on the *left*) (**a**) *black dash line*: spectrum of the Mn^{II}-tris-pyridyl-bis-amino complex (**b**) *blue plain lines*: spectra of recorded at different times during the formation of the MnOO intermediate (*arrows* indicate growing absorption with time). Adapted from [107]

Table 7.2 Superoxide $O_2^{\bullet-}$ consumed by reaction of KO_2 with Mn-complexes in anhydrous DMSO (eq./complex). See [97]

	$[Mn^{II}(TMIMA)_2]^{2+}$	$[Mn^{II}(IPG)(MeOH)]^{2+}$	$[Mn^{II}(BMPG)(H_2O)]^{2+}$	$[Mn^{II}(BIG)(H_2O)_2]^{2+}$	H_2O
Bound H_2O	0	0	1	2	–
Consumed O_2^-	1 eq.	1 eq.	3 eq.	5 eq.	0 eq.

that were characterized by their UV-vis and EPR characteristic 16-lines spectra [97]. The pathway leading to Mn^{III}-Mn^{IV}-di-μ-oxo structures is a dead-end for the catalysis of the superoxide dismutation and must be avoided for efficient SOD mimics with a high turnover. This dimerization into $Mn^{III}Mn^{IV}$ derivatives can be sterically precluded and indeed, in the case of coordinatively saturated Mn^{II} complexes—hexacoordination in $[Mn(TMIMA)_2]^{2+}$—or bulky ligands—picolyl moieties in BMPG—no dimer Mn^{III}–Mn^{IV}-di-μ-oxo was obtained upon reaction with superoxide [40].

The complexes in the series showed different hydration state, with complexes bearing zero, one, or two water molecules coordinated to the Mn^{II} ion. The consumption of superoxide as a function of this hydration level in anhydrous DMSO was studied, providing insight into the capacity of the complexes to cycle between the Mn^{II} and Mn^{III} redox states in the course of the reaction with superoxide [97]. As shown in Table 7.2, only one equivalent was consumed with $[Mn(TMIMA)_2]^{2+}$ and $[Mn^{II}(IPG)(MeOH)]^{2+}$ for which no water molecule was bound to the Mn^{II} ion. But with $[Mn^{II}(BIG)(H_2O)_2]^+$, isolated in water and bearing two coordinated water molecules, five equivalents of superoxide were consumed. With $[Mn^{II}(BMPG)(H_2O)]^{2+}$ three equivalents of superoxide were consumed. Note that water introduced in DMSO at the same concentration (that is twice that of the complex for a comparison with $[Mn^{II}(BIG)(H_2O)_2]^+$, and that of the complex for a comparison with $[Mn^{II}(BMPG)(H_2O)]^{2+}$) did not react efficiently with superoxide in the absence of complex. These observations clearly indicate the ability of the complexes from this series to react with superoxide with a stoichiometry higher than one when water is present. As rationalized in Fig. 7.10, the numbers of equivalent of superoxide consumed are consistent with the cycling between Mn^{II} and Mn^{III}.

In Water [40, 73, 97, 105, 106]

The reactivity with superoxide was studied in water using the indirect assay developed by McCord and Fridovich (see insert), which produces a slow and continuous flow of superoxide reminiscent of what is found in biological environments. All the complexes were found to be active, with kinetic constant k_{McCF} (see insert) of the order of 10^6–10^7 mol^{-1} L s^{-1}. The study in anhydrous conditions with different hydration levels suggested the ability of the complexes to react with superoxide with several turnovers. But, to ascertain their ability to be true SOD mimics and to catalytically dismutate superoxide, which is not straightforward with the Fridovich

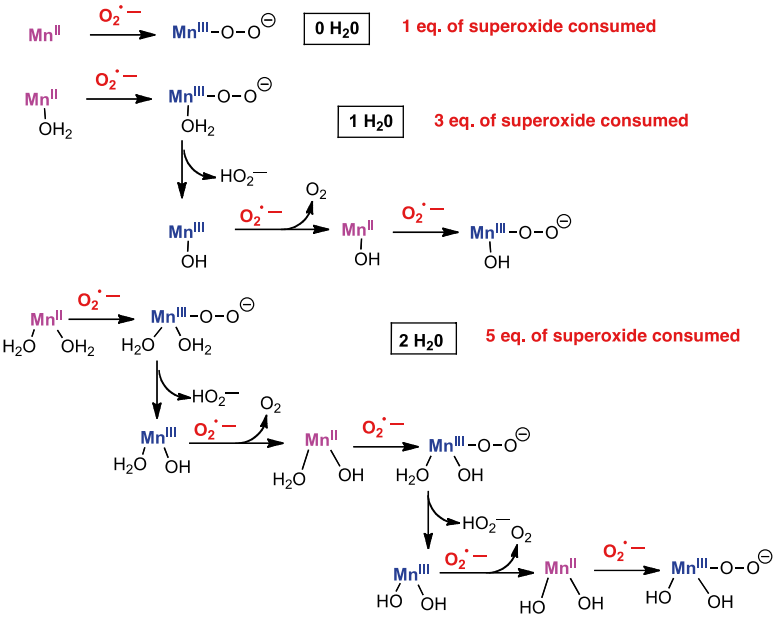

Fig. 7.10 Schematic rationale for the number of superoxide equivalents consumed in anhydrous DMSO upon the number of bound water molecules. See [97]

assay (see insert), reactivity was studied using pulsed radiolysis [40, 73]. A pulse of high concentration of superoxide can be produced in oxygenated aqueous solution in the presence of alcohol [121] upon irradiation. Superoxide disappearance in the presence of the SOD mimic at different concentrations can be followed at 270 nm ($\varepsilon = 1479$ L mol^{-1} cm^{-1}) [121–124]. Another way to investigate reactivity in large excess of superoxide is to use stopped-flow fast kinetic measurements with a highly concentrated solution of KO_2 in DMSO and rapid mixing in water [125]. Kinetic constants consistent with that from the McCord and Fridovich assay were obtained by pulsed radiolysis [40, 73] and more recently by stopped-flow [168].

Within this series, a correlation could be found between the kinetic constants derived from the McCord–Fridovich assay and the half-wave Mn^{III}/Mn^{II} potentials, with a negative slope (see Fig. 7.12, Δ markers). Within this series, as $E_{½}(Mn^{III}/Mn^{II}) > E_{midpoint}$, the SOD activity can be improved by lowering $E_{½}$ to $E_{midpoint}$, and hence by a stabilization of the Mn^{III} state [$E_{½}$ are defined as $(E_{anodic\ peak} + E_{cathodic\ peak})/2$]. Increasing the stabilization by imposing a Jahn–Teller distortion through a higher size metallacycle was efficient and led to the isolation of stable Mn^{III} complexes but poorer catalysts, probably because of an excessive Mn^{III} stabilization ($[Mn^{III}(PhI)_2]^+$ and $[Mn^{III}(PhIIm)_2]^+$, with (6) indicating a 6-membered metallacycle, see Fig. 7.8) [106].

These studies on the reactivity of these true SOD mimics were performed outside any cellular context and correspond to the intrinsic activity previously defined (see Sect. 7.2.4). As already mentioned, they are necessary, but not sufficient to ascertain bioactivity. Understanding and controlling inorganic compounds inside cells

requires new approaches to translating our knowledge in inorganic chemistry from the round-bottom flask into biological media and cells. Studies in bacteria or cells are still scarce, with the exception of SOD-deficient *E. coli* and *S. cerevisiae* that are potentially rescued by efficient SOD mimics [101, 126–128]. Recently, mammalian cellular models have emerged [108, 129, 130]. Macrophages are ideal cells to study SOD mimics under oxidative stress conditions. Interestingly, quantification of reactive oxygen species using an ultramicroelectrode can be performed at the single cell level [131]. One of the complexes of the SOD-inspired series, namely $[Mn^{II}(enPI^2)]^+$ (see Fig. 7.8), was shown to efficiently reduce the flow of reactive oxygen species (ROS) with a major reactivity toward the superoxide radical, evidenced through an assay using ferricytochrome *c* in the extracellular medium (extracellular McCord–Fridovich assay) [108].

7.4.2 Strategies to Control the Redox Potential

In the series presented above and directly inspired by the active site of MnSOD, the variation of activity ($\log(k_{cat})$) with redox potential shows a negative slope (see Fig. 7.12). Other groups have worked on the modulation of the redox potentials of Mn^{III}/Mn^{II} redox couple. Walton et al. have developed a series of Mn^{III} complexes based on a 1,3,5-triaminocyclohexane central scaffold, with three amino moieties in *cis* configuration that were grafted with *para*-substituted phenols (see Fig 7.11b). Mn^{III} complexes were isolated with octahedral Mn coordinated to three amine and three phenolato moieties [132]. The redox potentials, measured in DMF, were shown to vary over a volt with *para*-substituents such as methoxy, methyl, chloro, nitro [132], and tri-methylammonium [133]. The complexes were reported to display an SOD-like activity [133].

A thorough study regarding the effects of the modulation of the redox potential variation was performed by the group of Batinić-Haberle et al. For more than 15 years, they have been developing a large family of porphyrins, stable in aerobic conditions at the Mn^{III} state. They show a redox potential smaller than the redox mid-point optimal for superoxide dismutation, $E_{midpoint}$. In this case, increasing the redox potential goes with an increase in activity (see Fig. 7.12). Metalloporphyrins are interesting molecules for a chemist aiming to mimic biological structures. First, porphyrins are valuable and versatile structural scaffolds, with a large range of possible modifications at the *meso*- or ß-positions. In porphyrins bearing bulky substituents—*ortho*-functionalized phenyl, 2-*N*-alkylpyridyl, or *N*-alkyl-2-imidazolyl on the *meso*- position, see Fig. 7.11a—the substituents are perpendicular to the average porphyrin plane, with atropisomerism and the possibility of constructing a molecular scaffold above and below the porphyrin. This atropisomery has been used since the mid-1970s to develop superstructured porphyrins as mimics of hemoproteins [134–137]. In addition, the 3D-structure of these functionalized porphyrins renders them less prone to interaction with DNA [126], known to occur with more planar porphyrins, such as the *para*-substituted-pyridinium (see Mn^{III}TM-4-PyP^{5+} in

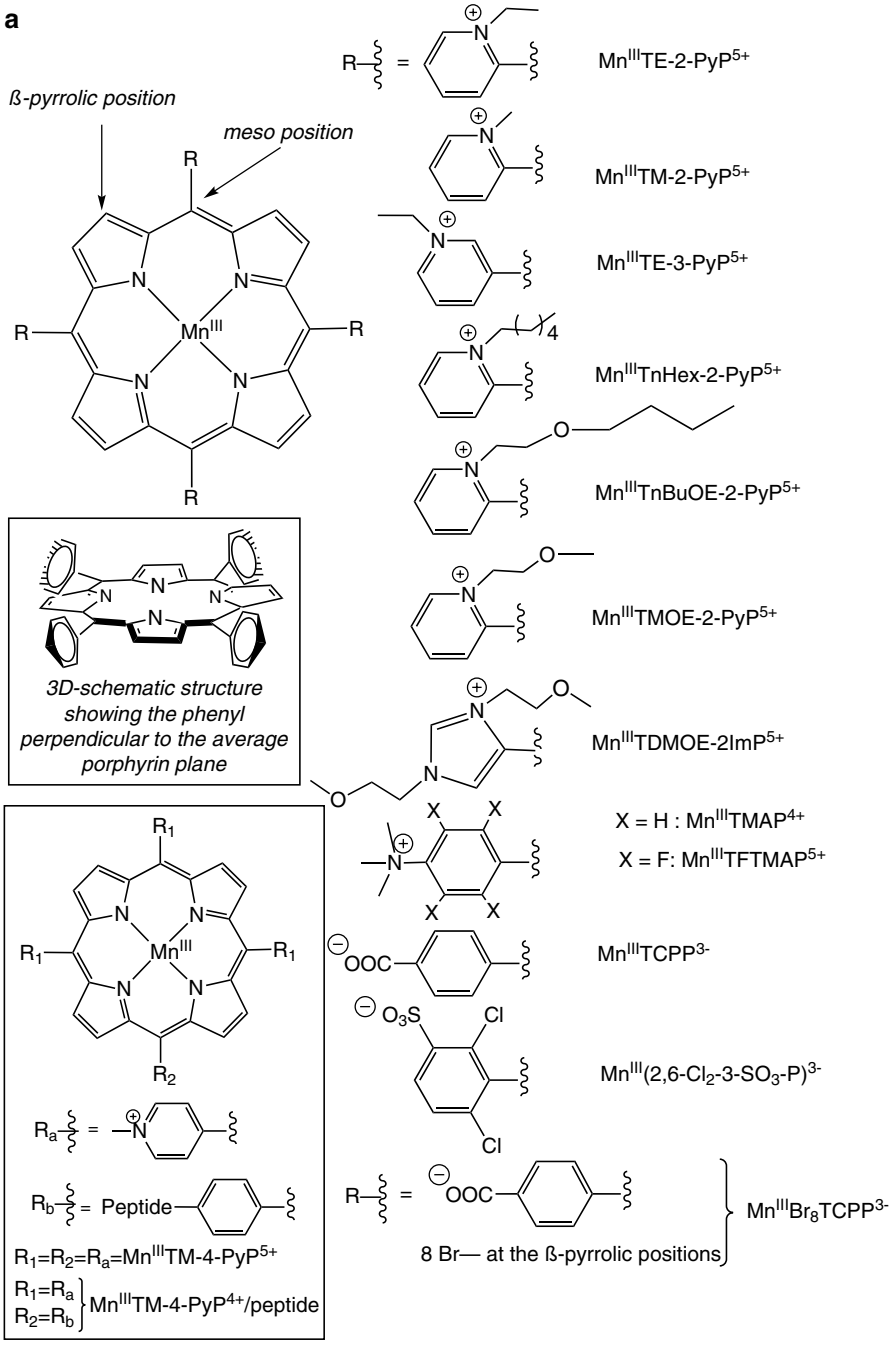

Fig. 7.11 (**a**) Structures of the Mn SOD mimics discussed in this chapter: structures of the Mn^{III} porphyrins. See: [23, 102, 126, 139, 141–144] and for Mn^{III}TM-4-PyP^{4+}/peptide see [126, 130, 142]. (**b**) Structure of the Mn SOD mimics discussed in this chapter: M40403 [99, 140], M40401, M40404 [140]; $Mn^{II}CnMe_2Pyane$ [145]; EUK207 [23]; Mn^{III}*cis*-TACH-N3O3 [133]; Mn^{II}(ABCDSA) [146]. Note that some Cl^- ligands have been seen in the solid state, but they are not shown here as there is most probably dissociation in water medium

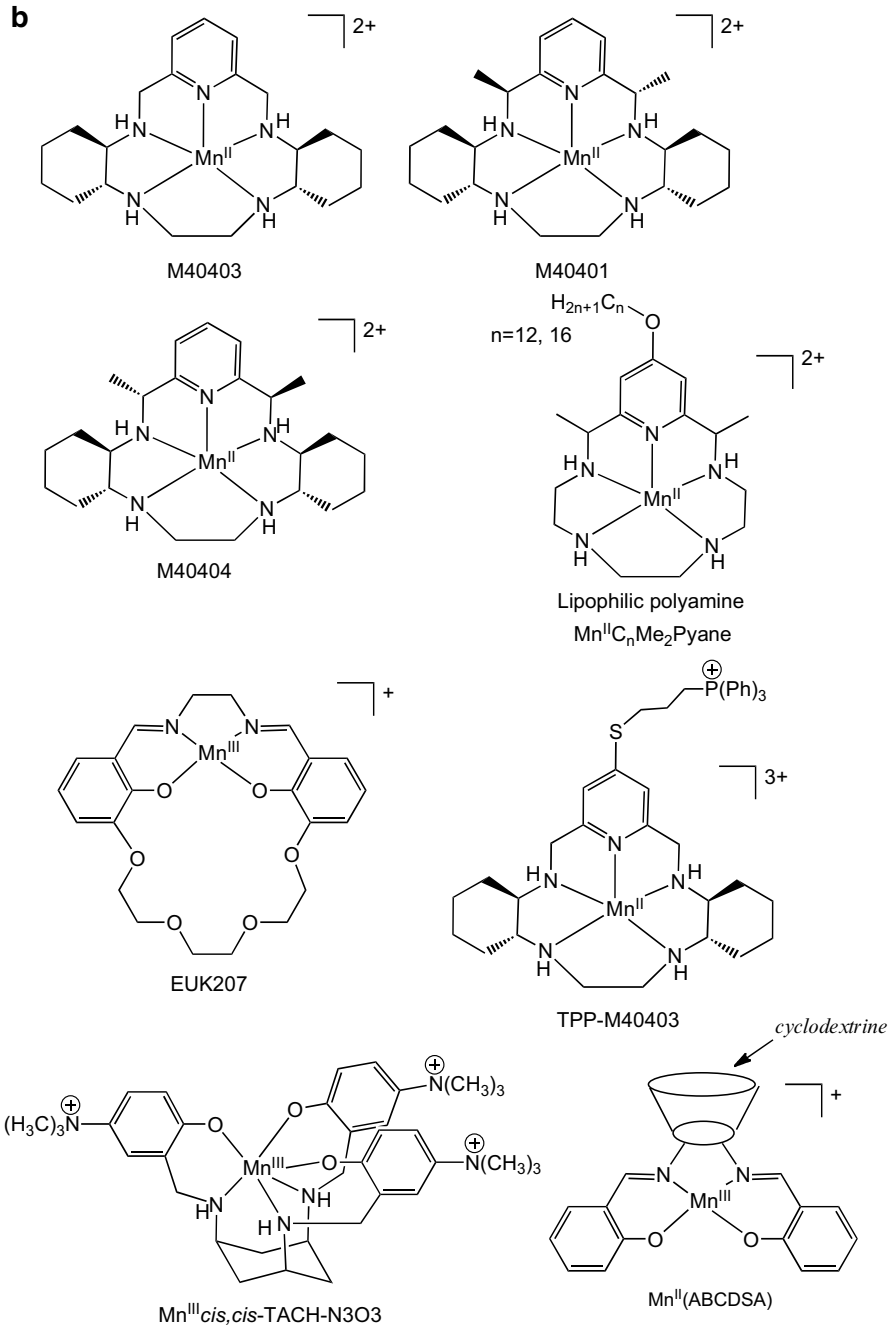

Fig. 7.11 (continued)

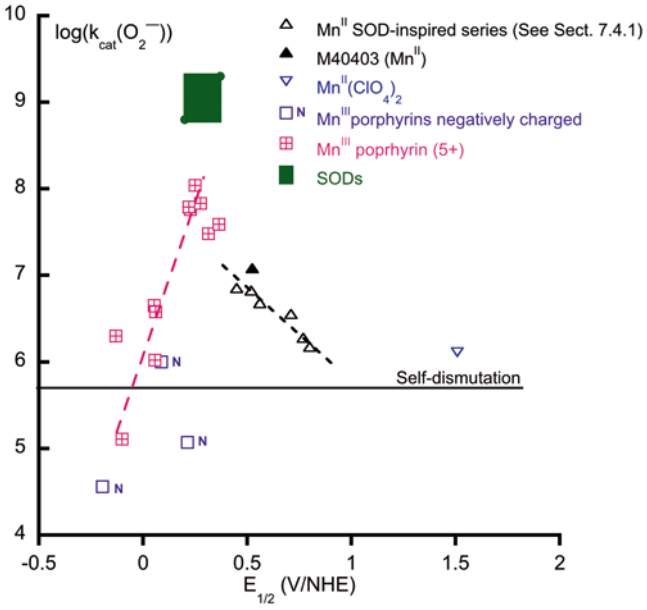

Fig. 7.12 Redox potentials (in water) and $\log k_{cat}(O_2^{-})$ for a series of Mn^{III}/Mn^{II} SOD mimics. *Triangles, up-ward*: Mn^{II} complexes directly inspired from SOD active site (see Sect. 7.4.1); *triangle, black*: M40403 (Mn^{II}); *triangle blue, down-ward*: $Mn^{II}(ClO_4)_2$ (Mn^{II}-hexa-aqua); *open-squares, purple N*: negatively charged porphyrins; *square with a cross, pink*: Mn^{III} porphyrins, 5+ charge. See Table 7.3 for the data and references. Inspired from [23, 40, 126, 139]

Fig. 7.11a, [138]). Porphyrins are efficient ligands, with high association constants and inertness for the metal complexes, although Mn has been shown to be lost in some rare cases for the reduced Mn^{II} form [23]. Electronic effects are easily propagated in these aromatic structures and redox potentials of the coordinated metal ions can be varied by functionalizing the porphyrin moiety with electroactive groups. Batinić-Haberle et al. prepared a wide series of Mn^{III} porphyrins showed to be true SOD mimics [23], using pulse radiolysis for instance [139]. Modulation of the redox potential over a wide range (800 mV) was achieved by functionalization with electron withdrawing groups (EWG) in *meso* or ß-positions, namely *N*-alkylpyridyl (PyP) or bis-*N*-alkylimidazolyl (ImP) groups (see Fig. 7.11a).

EWGs increase the electron deficiency on the metal center, which goes against oxidation into Mn^{III}. This favors low oxidation state and induces an increase in redox potential: the potential moves from negative values into the region of optimal $E_{½}$, i.e., to a redox potential which is closer to the $E_{midpoint}$. As expected, this variation was associated with an increase in activity, as shown in Fig. 7.12. Note that electrostatic effects are also important determinants of the activity and they will be discussed in Sect. 7.4.3.

Figure 7.12 shows dependence of $\log(k_{cat})$ as a function of $E_{½}$ for a series of SOD mimics based on Mn^{III}/Mn^{II} couples (see Table 7.3 for the data and references).

Table 7.3 Redox potentials of several manganese-SOD mimics based on a Mn^{III}/Mn^{II} redox couple

SOD mimics	$E_{½}$ (V vs. NHE)	Log k_{cat}	References
Mn^{III}TE-2-PyP^{5+}	0.228	7.76	[126]
Mn^{III}TM-2-PyP^{5}	0.220	7.79	[126]
Mn^{III}TE-3-PyP^{5+}	0.054	6.65	[23]
Mn^{III}TnHex-2-PyP^{3+}	0.314	7.48	[23]
Mn^{III}TnBuOE-2-PyP^{5+}	0.277	7.83	[23]
Mn^{III}TMOE-2PyP^{5+}	0.251	8.04	[139]
Mn^{III}TDMOE-2-ImP^{5+}	0.365	7.59	[139]
$Mn^{III}TCPP^{3-}$	–0.194	4.56	[126]
$Mn^{III}TFTMAP^{5+}$	0.058	6.02	[126]
$Mn^{III}TTMAP^{5+}$	–0.100	5.11	[126]
$Mn^{III}(2,6\text{-}Cl_2\text{-}3\text{-}SO_3\text{-}P)^{3-}$	0.088	6.00	[126]
Mn^{III}Br8$TCPP^{3-}$	0.213	5.07	[144]
Mn^{III}salen(EUK207)$^{+}$	–0.130	6.30	[23]
M40403 (Mn^{II})	0.525 (ACN)	7.08	[140]
M40404 (Mn^{II})	0.452 (ACN)	6.55	[140]
M40401 (Mn^{II})	0.464 (ACN)	Inactive	[140]
Mn^{III}*cis*-TACH-N3O3	0.31	5.95	[133]
$Mn^{II}(BIG)^{+}$	0.80	6.18	[40]
$Mn^{II}(IPG)^{+}$	0.77	6.28	[40]
$Mn^{II}(TMIMA)_2^{2+}$	0.71	6.55	[40]
$Mn^{II}(BMPG)^{+}$	0.56	6.68	[40]
$Mn^{III}(PI)_2^{+}$	0.52	6.82	[40]
$Mn^{II}(enPI_2)^{+}$	0.45	6.85	[105]
Self-dismutation	–	5.7	[23]
SOD	0.2–0.40	8.8–9.3	See Table 7.1
$Mn^{II}(ClO_4)_2$	1.51	6.11	[23, 40]

$E_{½} = (E_{anodic\ peak} + E_{cathodic\ peak})/2$

Mn^{III}/Mn^{II} SOD mimics can be classified into two subgroups, those displaying a redox potential smaller than $E_{midpoint}$ (0.36 V vs. NHE), which is the case of most Mn^{III} porphyrins and for which an increase in potential is favorable to the SOD activity, and those with a redox potential higher than $E_{midpoint}$, which is the case of the Mn^{II}-N_3O complexes previously described. Interestingly, for Mn^{III} porphyrins, the correlation $\log(k_{cat}) = f(E_{½})$ was shown to reflect the Marcus equation for outer-sphere electron exchanges [126, 139] with a tenfold increase for each 120 mV increase in $E_{½}$, suggesting an outer-sphere electron transfer.

In the case of the series of the cyclic polyamines series, it was found that the redox potentials of the Mn^{III}/Mn^{II} couples determined in ACN do not correlate with the activity (see M4040x in Fig. 7.11b and Table 7.3), suggesting a mechanism that does not involve SOD-like dismutation, but does involve the interaction superoxide with a Mn^{III}-peroxo intermediate [140].

Although the compounds presented in Fig. 7.12 are of quite different molecular structures (see Fig. 7.8 and 7.11a, b), with porphyrinic and 1,2-amino-based ligands, they fall on the same bell curve with a maximum activity recorded for compounds with a redox potential close to that of SOD, as expected. The correlation also extends to corroles or billiverdins through their Mn^{IV}/Mn^{III} redox potential, Fe^{III}/Fe^{II} porphyrins, stoichiometric scavengers such as nitroxides oxidized into oxo-ammonium, and Ce^{IV}/Ce^{III} in nanoparticles of cerium oxide (CeO_2) [23, 126, 128, 138, 139, 141]. These observations strengthen, if necessary, the idea that activity can be optimized by tuning the redox potential.

7.4.3 *Electrostatic Attraction and Other Effects Modulating the Intrinsic Activity*

All the pairs ($E_{½}$, $\log(k_{cat})$) do not fall exactly on the correlation in Fig. 7.12. The scatter reflects factors other than the thermodynamic $E_{1/2}$ impacting the reactivity, such as electrostatic effects, shape, or local dipolar effects [23, 142, 144]. Electrostatic effects associated with superoxide attraction and interplay with the lipophilicity inducing solvation/desolvation effects come into play to modulate the redox potential [139, 144].

An exception in the previous correlation is seen in Fig. 7.12 with the negatively charged Mn^{III} porphyrins. For instance, the porphyrin $[Mn^{III}Br_8TCPP]^{3-}$ shows a redox potential for the Mn^{III}/Mn^{II} redox couple very close to that of $[Mn^{III}TE\text{-}2\text{-}PyP]^{5+}$ but with a kinetic constant 100-fold smaller. This was rationalized by an impaired interaction between the negatively charged porphyrin and the negatively charged superoxide [142].

In the case of the porphyrins series developed by Batinić-Haberle et al., the quaternarization of the pyridyl and imidazolyl in the ortho position, leading to positively charged pyridinium or imidazolium moieties conjugated with alkyl or polyether chains, was proven to be quite a valuable strategy with cumulative favorable effects [23]. In this series of positively charged Mn^{III} porphyrins with *N*-alkyl in *ortho*-position and for each individual Mn^{III} porphyrin, a decrease in k_{cat} upon increase in ionic strength (I) was observed with linear correlation between $\log(k_{cat})$ and $\frac{\sqrt{I}}{1+\sqrt{I}}$ [139, 142, 147]. This observation, similar to that observed for proteins themselves, clearly reveals a favorable electrostatic interaction between the negatively charged superoxide and the positive Mn^{III} porphyrins catalysts that is shielded when I increases. A very weak dependence of k_{cat} on I was recorded in the case of *para* and *meta*-substituted porphyrin [142]. This brings out the role of the charge topography: with *ortho*-alkylpyridinium ($Mn^{III}TE\text{-}2PyP^{5+}$), the charge is distributed over a donut above the metal center mimicking closely the topography of the funnel in the proteins. In contrast, with the *para*-alkylpyridinium ($Mn^{III}TM\text{-}4PyP^{5+}$), attraction is that of an overall charge distributed at the far periphery of the porphyrin,

which was proven to be less efficient and a much weaker shielding is observed with increase in ionic strength [142]. It appears thus that it is necessary, in this biomimetic or bioinspired approach, to reproduce not only the charges but also their topology, with attraction along a funnel [147]. Recently, the SOD bio-inspired series (see Sect. 7.4.1) was conjugated to oligo-arginine moieties, with 1, 3, 6 and 9 Arg. Analyses of the dependence of the k_{cat} with ionic strenght showed that only the two or three first arginines were effective in the enhancement of k_{cat} associated with an electrostatic effect. This was rationalized by the fact that the long peptide chain was most probably topologically disordered [168]. These examples are reminiscent of the double topographic effect suggested above in the case of SODs: their overall negative charge repels the superoxide ion towards the attractive positively charged funnel (see Sect. 7.3.2 and Fig. 7.5).

Some interesting local effects have also been observed with porphyrins functionalized with alkyl and ether chains. More lipophilic porphyrins were found less sensitive to changes in ionic strength, revealing the importance of local dielectric environment [139]. This is an important consideration also for proteins, for which dielectric constants are not uniform but modulated by the amino acid side chains nearby. In addition, porphyrins functionalized with ether groups were found to display higher kinetic constants (see Table 7.3) with a stronger dependence on ionic strength, probably associated with a higher solvation [139]. As observed in the 1980s in the course of mimicking myoglobin with iron porphyrins [135], ether groups, able to accept hydrogen bonds, either from Fe-hydroperoxo adduct or from water, create a local hydration [139] that can play a role in superoxide dismutation especially in the reduction reaction, for which protons are necessary.

7.4.4 Bioavailability and Localization

Bioavailability and cellular distribution are also strong determinants of the bioactivity of the SOD mimics [23]. Water insolubility can be an issue preventing bioactivity from being revealed, and strategies have been developed to improve water solubility. In parallel, the complexes need to efficiently penetrate into cells, which requires amphiphilic properties.

Several groups have developed strategies to conjugate SOD mimics with moieties favoring water solubility. A Mn^{III} salen complex was built onto a cyclodextrin (CD) scaffold to efficiently improve the solubility and to take advantage of the CD $HO^{\bullet}$-scavenging properties (MnABCDSA, see Fig. 7.11b, [146]). Functionalization of porphyrins by negatively charged moieties, such as sulfonato in $Mn^{III}(2,6\text{-}Cl_2\text{-}3\text{-}SO_3\text{-}P)^{3-}$, or carboxylato in $Mn^{III}TCCP^{3-}$, meant to provide good water solubility, is detrimental for electrostatic attraction of superoxide, as discussed above [144]. In contrast, quaternarization of the pyridyl or imidazolyl moieties leads to efficient water-soluble positively charged SOD mimics, with redox potential tuned by the strong electrowithdrawing properties of pyridinium and imidazolium groups [23]. Increasing the amphiphilicity by long alkyl chains was shown to be favorable for the bioavailability and therapeutic efficacy, but some toxicity associated with

detergent effect was observed at concentrations lower than that of lower-alkyl-chain analogs [128]. Interestingly, substituting the long alkyl chains with ether chains led to an increased intrinsic activity (k_{cat}), probably due to a solvation cavity and local polarity with an efficiency to restore normal growth in SOD-deficient yeast [143].

In a similar approach aimed at modulating lipophilicity, Mn^{II}-cyclic polyamine complexes were conjugated with long alkyl chains in $Mn^{II}C_nMe_2Pyane$ [145]. The authors showed a tendency of the resulting compounds to form aggregates or micelles. Despite a lower thermodynamic stability and a lower reactivity toward superoxide, as determined by stopped-flow measurements, in comparison with the unsubstituted analog, cell studies revealed a beneficial effect on preventing lipid peroxidation at low concentration of the lipophilic complex [145].

Para-substituted pyridinium porphyrins (Mn^{III}TM-4-PyP^{5+}) were also associated with a catalase-polyethyleneglycol (cat-PEG) moiety [148, 149] with the double objective of enhancing the Mn^{III} porphyrin half-life in blood circulation and conjugating SOD with catalase activity for antioxidative stress applications in the plasma, such as ischemia-reperfusion injuries. In these physiopathological conditions, ROS are produced when blood circulation is re-established again in a de-perfused tissue, causing oxidative damages to proteins and lipid membranes.

Cellular recognition is also a key parameter of bioactivity. M40403 was conjugated to a galactose moiety [150] to encourage interaction with lectins, proteins that play an important role in recognition processes at the cell-membrane surface. Porphyrins functionalized with lactose were also developed with the same goal [151].

Intracellular targeting to mitochondria can be favorable for bioactivity, since superoxide potential overproduction occurs primarily in mitochondria. Asayama et al. have developed a porphyrin functionalized with a mitochondria-targeting peptide (Mn^{III}TM-4-PyP-$peptide^{n+}$), which showed a sixfold decrease in k_{cat} in comparison with the unsubstituted porphyrin (1.8×10^6 and 11×10^6 mol^{-1} L s^{-1}, respectively, measured by stopped-flow technique), but with mitochondrial accumulation. Protection against lipopolysaccharide toxicity on murine macrophages was more efficient than with the non-conjugated analog [130].

More generally, Mn^{III} porphyrins developed by Batinić-Haberle et al. are positively charged, exhibiting hydrophobic to amphiphilic characteristics and spontaneous accumulation at mitochondria [102], which was suggested as the reason for their efficiency in restoring growth in SOD-deficient *E. coli* and yeast mutants (see Sect. 7.4) [101].

Smith and Murphy have functionalized antioxidants like vitamin E with triphenylphosphonium moieties showing strong accumulation at mitochondria [93]. Recently, they have functionalized M40403 (TPP-M40403) with the same moiety [152]. The resulting derivative showed an intrinsic activity tenfold higher than the non-conjugated M40403, a 3000-fold accumulation in isolated mitochondria with an efficiency to protect mitochondrial aconitase from inactivation upon paraquat stress [152].

The subcellular distribution of MnSOD mimics are actually key to the antioxidant activity and new techniques are emerging to better characterize them [153]. These are important directions for future research in this field.

7.5 Conclusion

Superoxide dismutases are proteins that have been gradually carved by evolution to perform very effective catalysis of the superoxide dismutation aimed at protecting cells against damages from oxidative stress associated with superoxide. On the one hand, understanding the determinants for efficient activity at the molecular level is an important fundamental challenge. Tuning of redox potential, metal selectivity (not discussed here, see [1, 65]), and electrostatic attraction are crucial characteristics and mechanisms involved in SODs that have been analyzed along the years. On the other hand, in a bioinspired approach, chemists have taken advantage of what has been understood from these mechanisms to convey and apply them to the design of efficient catalysts for superoxide dismutation, with potential therapeutic perspective. This

Intrinsic Activity of SOD Mimics: Assays for SOD Activity in Water
The evaluation of the reaction kinetics of superoxide with a putative SOD mimic can be performed using direct or indirect tests. In the indirect methods, superoxide is provided at a constant rate and at concentrations close to what is encountered in biological systems under oxidative stress, providing a test for the ability of the putative SOD mimic to be useful in physiological conditions. However, in some cases it is difficult to distinguish between a catalyst and a scavenger (see below). In direct methods, since superoxide can be provided in large excess in comparison to the putative SOD mimic, unambiguous characterization of a catalyst versus a scavenger can be obtained.

Indirect assay: **McCord and Fridovich test**
The paradigmatic indirect assay is the McCord Fridovich test, which was originally set up to establish the activity of SOD [51]. In indirect assays, a continuous flow of superoxide is produced, usually by an enzymatic system, as in the McCord–Fridovich test: xanthine-oxidase oxidizes xanthine to urate, with specific conditions (pH, O_2) chosen in order to maximize the re-oxidation of the reduced enzyme with the release of superoxide [154]. The assay is based on a kinetic competition between the putative SOD mimic or SOD itself and a redox indicator that changes in color upon reacting with superoxide. The UV-vis. indicator is necessary since the flow in superoxide (1.2 μM min^{-1} [155]) is too low and the absorption coefficient of superoxide too weak to enable a direct spectrophotometric detection. The most frequently used indicators are cytochrome *c* Fe^{III} reduced in cytochrome *c* Fe^{II}, or nitro-blue tetrazolium (NBT)

reduced into formazan. Because NBT is not very soluble new tetrazolium salts leading to more soluble formazan forms have been developed [156]. A 50 % inhibition concentration (*IC50*) is determined, which corresponds to the concentration in the SOD mimic or SOD that reduces by 50 % the speed of the reduction of the indicator. *IC*50 values are dependent both on the nature of the indicator used and on its concentration: for a given putative SOD mimic, the smaller the detector concentration, the smaller the *IC*50 value. An important consequence is that *IC*50 values are not appropriate for comparisons across the literature. But from the measured *IC*50 values, an apparent kinetic constant value (k_{McCF}) can be calculated, which is independent of both the concentration and the nature of the detector [40].

At the *IC*50 concentration, superoxide reacts at the same speed with the detector and the putative SOD mimic:

$$k_{McCF} \cdot IC50 \cdot \left[O_2^{\bullet -}\right] = k_{detector} \cdot [detector] \cdot \left[O_2^{\bullet -}\right]$$

Then, $k_{McCF} = k_{detector} \cdot [detector]/IC50$ [40, 157].

In the case of cytochrome *c* Fe^{III} as the detector, $k_{Cyt\ c}$ (pH = 7.8; 21 °C) = 2.6×10^5 mol^{-1} L s^{-1} [158]. In the case of NBT, k_{NBT} (pH = 7.8) = 5.94×10^4 mol^{-1} L s^{-1} [159].

Reliability of the McCord–Fridovich Assay [40, 160, 161]:
It is necessary to check that the putative SOD mimic does not inhibit the production of superoxide by xanthine oxidase. This can be performed by the determination of the rate of conversion of xanthine to urate. The putative SOD mimic should not react with ferri or ferrocytochrome *c*. Ideally, this should be checked for both redox states of the SOD mimic, but is not always possible.

A second important point to consider is the steady state in superoxide in this assay. Under canonical conditions, the test produces about 1.2 μM min^{-1} [155] and lasts about 10 min [162]. During this 10-min period, 12 μM of superoxide will have been produced and half of the superoxide has reacted with cytochrome *c* Fe^{III} and half with the putative SOD mimic. Hence, at *IC50* higher than 6 μM, the turnover of the SOD mimic in the experiment performed at the *IC50* concentration is not more than one. To ensure a catalytic nature would require high turnover number and this is obtained for *IC50* much smaller than μM. This is the case with SOD but generally not for most SOD mimics.

The cyt *c* assay has been shown to be free of artifacts in the large majority of cases and worked with a wide range of SOD mimics tested so far and its validity has been checked by stopped-flow and pulse radiolysis [73, 163]. The frequently used NBT (nitrobluetetrazolium) assay has artifacts as the assay also produces superoxide [164]. Moreover, NBT can be reduced to NBT$^{\bullet}$ radical (which disproportionates to blue formazan) by superoxide and numerous

enzymes as well as by nonenzymatic reductants [165]. Thus, the assay with NBT is not superoxide specific. Once reduced, $NBT^{\bullet}$ radical can be oxidized back with oxygen-producing superoxide and regenerating NBT, which would falsely suggest that NBT reduction is inhibited. Good controls as well as expressing the activity in terms of rate constants (see above) and not *IC50* is important to have meaningful data readily available. For comparison with literature data on available SOD mimics, one needs to express results on SOD-like activity in terms of rate constants and not in terms of *IC50* values.

Direct assays
Direct methods, which test the activity at a superoxide concentration that is much higher than the SOD mimic concentration, are important in ascertaining the catalytic nature of an SOD mimic. Two main techniques can be used. The first one consists of rapid mixing of solution in high superoxide concentration (typically KO_2 in DMSO or ACN) using a stopped-flow system [125, 166, 167]. The superoxide radical can also be produced in oxygenated aqueous solutions by pulsed radiolysis [122–124]. High-energy ionizing radiation generates primary radicals (H, e^-_{aq}, $HO^{\bullet}$) that are rapidly and quantitatively converted into either superoxide $O_2^{\bullet-}$ or its protonated form hydroperoxyl $HO_2^{\bullet}$, in the presence of either formate or alcohols, since formate might coordinate to manganese [61, 121]. See for example: [40, 73].

Concluding remark: In the indirect methods, superoxide is provided at a constant slow rate and at concentrations close to that encountered in biological systems. This provides a test for the ability of a putative SOD mimic to be useful under physiological situations. However, in most cases it is difficult to distinguish between a catalyst and a scavenger. With the direct methods, since superoxide can be used in large excess relative to the putative SOD mimic, unambiguous characterization of an SOD mimic as a catalyst or a scavenger can be obtained. Indirect and direct methods are thus complementary [56, 73].

is at the very heart of the bioinspired approach, with dual interest: to develop chemical models to improve the understanding of physicochemical processes in natural systems, and also to learn lessons from Nature to generate efficient artificial systems. SOD mimic designing is a paradigmatic field in realizing these goals.

References

1. Sheng Y, Abreu IA, Cabelli DE, Maroney MJ, Miller A-F, Teixeira M, Valentine JS. Superoxide dismutases and superoxide reductases. Chem Rev. 2014;114:3854–918.
2. Sessions AL, Doughty DM, Welander PV, Summons RE, Newman DK. The continuing puzzle of the great oxidation event. Cur Biol. 2009;19(14):R567–74.
3. Pierre J-L, Crichton RR. Old iron, young copper: from Mars to Venus. BioMetals. 2001;14:99–112.

4. Valentine JS. Dioxygen reactivity and toxicity. In: Bertini I, Gray SJ, Stiefel EI, Valentine JS, editors. Biological inorganic chemistry, structure and reactivity. Mill Valley: University Science Books; 2007. p. 319–31.
5. Koppenol WH. Oxygen activation by cytochrome P450: a thermodynamic analysis. J Am Chem Soc. 2008;129:9686–90.
6. Que LJ. Dioxygen activating enzymes. In: Bertini I, Gray SJ, Stiefel EI, Valentine JS, editors. Biological inorganic chemistry, structure and reactivity. Mill Valley: University Science Books; 2007. p. 388–413.
7. Koppenol WH, Stanbury DM, Bounds PL. Electrode potentials of partially reduced oxygen species, from dioxygen to water. Free Radical Biol Med. 2010;49:317–22.
8. Kirkinezosa IG, Moraesa CT. Reactive oxygen species and mitochondrial diseases. Semin Cell Dev Biol. 2001;12:449–57.
9. Halliwell B, Gutteridge JMC. Free radicals in biology and medicine. New York: Oxford University Press; 2007.
10. Goldberg IH. Mechanism of neocarzinostatin action: role of DNA microstructure in determination of chemistry of bistranded oxidative damage. Acc Chem Res. 1991;91(7):191–8.
11. Dix TA, Hess KM, Medina MA, Sullivan RW, Tilly SL, Webb TLL. Mechanism of site-selective DNA nicking by the hydrodioxyl (perhydroxyl) radical. Biochemistry. 1996;35(14):4578–83.
12. Nelson SK, Bose SK, McCord JM. The toxicity of high-dose superoxide dismutase suggests that superoxide can both initiate and terminate lipid peroxidation in the reperfused heart. Free Radical Biol Med. 1994;16:195–200.
13. Gardner PR, Fridovich I. Superoxide sensitivity of the Escherichia coli 6-phosphogluconate dehydratase. J Biol Chem. 1991;266:1478–83.
14. Gardner PR, Fridovich I. Inactivation-reactivation of aconitase in E. coli: a sensitive measured of superoxide radical. J Biol Chem. 1992;267:8757–63.
15. Gardner PR, Raineri I, Epstein LB, White CW. Superoxide radical and iron modulate aconitase activity in mammalian-cells. J Biol Chem. 1995;270:13399–405.
16. Charrier JG, Anastasio C. Impacts of antioxidants on hydroxyl radical production from individual and mixed transition metals in a surrogate lung fluid. Atmos Environ. 2011;45: 7555–62.
17. Iranzo O. Manganese complexes displaying superoxide dismutase activity: a balance between different factors. Bioorg Chem. 2011;39:73–87.
18. Aguirre JD, Culotta VC. Battles with iron: manganese in oxidative stress protection. J Biol Chem. 2012;287:13541–8.
19. Theil EC. Ferritin. In: Bertini I, Gray SJ, Stiefel EI, Valentine JS, editors. Biological inorganic chemistry, structure and reactivity. Mill Valley: University Science Books; 2007; p. 144–50.
20. Holley AK, Dhar SK, Xu Y, St. Clair DK. Manganese superoxide dismutase: beyond life and death. Amino Acids. 2012;42(1):139–58.
21. Inoue M, Sato EF, Nishikawa M, Park AM, Kira Y, Imada I, Utsumi K. Mitochondrial generation of reactive oxygen species and its role in aerobic life. Curr Med Chem. 2003;23:2495–505.
22. McCord JM, Edeas MA. SOD, oxidative stress and human pathologies: a brief history and a future vision. Biomed Pharmacother. 2005;59:139–42.
23. Batinic-Haberle I, Tovmasyan A, Roberts ER, Vujaskovic Z, Leong KW, Spasojevic I. SOD therapeutics: latest insight into their structure-activity relationships and impact on the cellular redox-based signaling pathways. Antioxid Redox Signal. 2014;20(15):2372–415.
24. Batinic-Haberle I, Reboucas Julio S, Spasojevic I. SOD mimic: chemistry, pharmacology and therapeutic potential. Antioxid Redox Signal. 2010;13(6):877–918.
25. Muscoli C, Cuzzocrea S, Riley DP, Zweier JL, Thiemermann C, Wang ZQ, Salvemini D. On the selectivity of SOD mimetics and its importance in pharmacological studies. Br J Pharmacol. 2003;140:445–60.

26. Salvemini D, Muscoli C, Riley DP, Cuzzocrea S. Superoxide dismutases mimetics. Pulm Pharmacol Ther. 2002;15:439–47.
27. Fridovich I, Imlay JA. Assay of metabolic superoxide production in Escherichia coli. J Biol Chem. 1991;266:6957–65.
28. Melov S, Coskun P, Patel M, Tuinstra R, Cottrell B, Jun AS, AZastawny TH, Dizdaroglu M, Goodman SI, Huang TT, Miziorko H, Epstein CJ, Wallace DC. Mitochondrial disease in superoxide dismutase 2 mutant mice. Proc Natl Acad Sci U S A. 1999;96:846–51.
29. Li Y, Huang T-T, Carlson EJ, Melov S, Ursell PC, Olson JL, Noble LJ, Yoshimura MP, Berger C, Chan PH, Wallace DC, Epstein CJ. Dilated carbiomyopathy and neonatal lethality in mutant mice lacking MnSOD. Nat Genet. 1995;11:376–81.
30. Reaume AG, Elliott JL, Hoffman EK, Kowall NW, Ferrante RJ, Siwek DR, Wilcox HM, Flood DG, Beal MF, Brown Jr RH, Scott RW, Snider WD. Motor neurons in Cu/Zn superoxide dismutase-deficient mice develop normally but exhibit enhanced cell death after axonal injury. Nat Genet. 1996;13:43–7.
31. Yost FJ, Fridovich I. An iron-containing superoxide dismutase from Escherichia coli. J Biol Chem. 1973;248(14):4905–8.
32. Youn H-D, Kim E-J, Roe J-H, Hah YC, Kang SO. A novel nickel-containing superoxide dismutase from Streptomyces spp. Biochem J. 1996;318:889–96.
33. Niviere V, Fontecave M. Discovery of superoxide reductase: an historical perspective. J Biol Inorg Chem. 2004;9:119–23.
34. Austin FE, Barbieri JT, Crorin RE, Grigas KE, Cox CD. Distribution of superoxide dismutase, catalase, and peroxidase activities among Treponema pallidum and other spirochetes. Infec Immun. 1981;33(2):372–9.
35. Archibald FS, Fridovich I. Mn and defenses against oxygen toxicity in Lactobacillus plantarum. J Bacteriol. 1981;445:442–51.
36. Seib KL, Tseng H-J, McEwan AG, Apicella MA, Jennings MP. Defenses against oxidative stress in Neisseria gonorrhoeae and Neisseria meningitidis: distinctive systems for different lifestyles. J Infect Disease. 2004;190:136–47.
37. Jones DP, Go YM, Anderson CL, Ziegler TR, Kinkade JM, Kirlin WG. Cysteine/cystine couple is a newly recognized node in the circuitry for biologic redox signaling and control. Faseb J. 2004;18(9):1246–8.
38. Latour J-M. Manganese, the stress reliever. Metallomics. 2015;7:25–8.
39. Archibald FS, Fridovich I. The scavenging of superoxide radical by manganous complexes: in vitro. Arch Biochem Biophys. 1982;214:452–63.
40. Durot S, Policar C, Cisnetti F, Lambert F, Renault J-P, Pelosi G, Blain G, Korri-Youssoufi H, Mahy J-P. Series of Mn complexes based on N-centered ligands and superoxide—reactivity in an anhydrous medium and SOD-like activity in an aqueous medium correlated to Mn^{II}/Mn^{III} redox potentials. Eur J Inorg Chem. 2005;3513–23.
41. Barnese K, Gralla EB, Cabelli DE, Valentine JS. Manganous phosphate acts as a SOD. J Am Chem Soc. 2008;130:4604–6.
42. McNaughton RL, Reddi AR, Clement MHS, Sharma A, Barnese K, Rosenfeld L, Butler Gralla E, Valentine JS, Culotta VC, Hoffman B. Probing in vivo Mn2+ speciation and oxidative stress resistance in yeast cells with electron-nuclear double resonance spectroscopy. Proc Natl Acad Sci U S A. 2010;107(35):15335–9.
43. Reddi AR, Culotta VC. Regulation of manganese antioxidants by nutrients sensing pathway in saccharomyces cerevisiae. Genetics. 2011;189:1261–70.
44. Mann T, Keilin D. Haemocuprein and hepatocuprein, copper protein compounds of blood and liver in mammals. Proc R Soc Ser B. 1938;126:303–15.
45. Markowitz H, Cartwright GE, Wintrobe MM. Studies on copper metabolism: XXVII. An Erythrocyte cuproprotein. The isolation and properties of an erythrocyte cuproprotein (erythrocuprein). J Biol Chem. 1959;234:40–5.
46. Pauling L. The discovery of superoxide radical. Trends Biochem Sci. 1979;4(11):N270–1.
47. Pauling L. The nature of the chemical bond. IV The energy of single bonds and the relative electronegativity of atoms. J Am Chem Soc. 1932;54:3570–82.

48. Neuman EW. Potassium superoxide and the three-electron bond. J Chem Phys. 1934;2:31–3.
49. Bray RC, Knowles PF. Electron spin resonance in enzyme chemistry: the mechanism of action of xanthine oxidase. Proc Roy Soc A. 1968;302:351–53.
50. Knowles PF, Gibson JF, Pick FM, Bray RC. Electron-spin-resonance evidence for enzymic reduction of oxygen to a free radical, the superoxide ion. Biochem J. 1969;111:53–8.
51. McCord JM, Fridovich I. Superoxide dismutase. An enzymatic function for erythrocuprein (hemocuprein). J Biol Chem. 1969;244(22):6049–55.
52. Carson S, Vogin EE, Huber W, Schulte TL. Safety tests of orgotein, an antiinflammatory protein. Toxicol Appl Pharmacol. 1973;26:184–202.
53. Babior BM, Kipnes RS, Curnutte JT. The production by leukocytes of superoxide radical, a potential bactericial agent. J Clin Invest. 1973;52:741–4.
54. Miriyala S, Spasojevic I, Tovmasyan A, Salvemini D, Vujaskovic Z, St. Clair D, Batinic-Haberle I. MnSOD and its mimic. Biochim Biophys Acta. 2012;1822(5):794–814.
55. Axthelm F, Casse O, Koppenol WH, Nauser T, Meier W, Palivan CG. Antioxidant nanoreactor based on SOD encapsulated in SOD permeable vesicles. J Phys Chem B. 2008;112(28):8211–6.
56. Riley DP. Functional mimics of superoxide dismutase enzymes as therapeutic agents. Chem Rev. 1999;99:2573–87.
57. Salvemini D, Riley DP, Cuzzocrea S. SOD mimetics are coming of age. Nat Rev Drug Discov. 2002;1(5):367–74.
58. Abreu IA, Cabelli DE. Superoxide dismutases—a review of the metal-associated mechanistic variations. Biochim Biophys Acta. 2010;1804:263–74.
59. Basolo F, Pearson RG. Mechanisms of inorganic reactions: a study of metal complexes in solution. New York: Wiley; 1967.
60. Barrette WCJ, Sawyer DT, Fee JA, Asada K. Potentiometric titration and oxidation-reduction potentials of several iron superoxide dismutases. Biochemistry. 1983;22(3):624–7.
61. Bielski BHJ, Cabelli DE, Arudi RL, Ross AB. Reactivity of HO_2/O_2^- radicals in aqueous solution. J Phys Chem Ref Data. 1985;14(4):1041–100.
62. Azab HA, Banci L, Borsari M, Luchinat C, Sola M, Viezzoli MS. Redox chemistry of superoxide-dismutase- Cyclic voltammetry of wild-type enzymes and mutants on functionally relevant residues. Inorg Chem. 1992;31(22):4649–55.
63. Lawrence GD, Sawyer DT. Potentiometric titrations and oxidation-reduction potentials of manganese and copper-zinc superoxide dismutases. Biochemistry. 1979;19:3045–50.
64. Herbst RW, Guce A, Bryngelson PA, Higgins KA, Ryan KC, Cabelli DE, Garman SC, Maroney MJ. Role of conserved tyrosine residues in NiSOD catalysis: a case of convergent evolution. Biochemistry. 2009;48(15):3354–69.
65. Miller A-F. Redox tuning over almost 1 V in a structurally conserved active site: lessons from Fe-containing superoxide dismutase. Acc Chem Res. 2008;41(4):501–10.
66. Marshall NM, Garner DK, Wilson TD, Gao Y-G, Robinson H, Nilges MJ. Rationally tuning the reduction potential of a single cupredoxin beyond the natural range. Nature. 2009;462:113–7.
67. New SY, Marshall NM, Hor TSA, Xue F, Lu Y. Redox tuning of biological copper centers through non-covalent interactions: same trends but different magnitude. Chem Commun. 2012;48:4217–9.
68. Drew MGB, Harding CJ, McKee V, Morgan GG, Nelson J. Geometric control of manganese redox state. J Chem Soc Chem Commun. 1995;10:1035–8.
69. Garcia L, Cisnetti F, Gillet N, Guillot R, Aumont-Nicaise M, Piquemal J-P, Desmadril M, Lambert F, Policar C. Entasis through Hook-and-Loop factening in a glycoligand with cumulative weak forces stabilizing Cu(I). J Am Chem Soc. 2015;137(3):1141–6.
70. Suh J, Chei WS. Metal complexes as artificial proteases: toward catalytic drugs. Curr Opin Chem Biol. 2008;12:207–13.
71. Lombard M, Fontecave M, Touati D, Nivière V. Reaction of the desulfoferrodoxin from Desulfoarculus baarsii with superoxide anion—Evidence for a superoxide reductase activity. J Biol Chem. 2000;275:115–21.

72. Pianzzola MJ, Soubes M, Touati D. Overproduction of the rbo gene product from Desulfovibrio species suppresses all deleterious effects of lack of superoxide dismutase in Escherichia coli. J Bacteriol. 1996;178:6736–42.
73. Durot S, Lambert F, Renault J-P, Policar C. A pulse radiolysis study of superoxide radical catalytic dismutation by a manganese(II) complex with a N-tripodal ligand. Eur J Inorg Chem. 2005;2789–93.
74. Quinn R, Mercer-Smith J, Burstyn JN, Valentine JS. Influence of hydrogen bonding on the properties of iron porphyrin imidazole complexes. An internally hydrogen bonded imidazole ligand. J Am Chem Soc. 1984;106:4136–44.
75. Haga M-A, Ano T-A, Kano K, Yamabe S. Proton-induced switching of metal-metal interactions in dinuclear ruthenium and osmium complexes bridged by 2,2′-bis(2-pyridyl)-bibenzimidazole. Inorg Chem. 1991;30:3843–9.
76. Carina RF, Verzegnassi L, Bernadinelli G, Williams AF. Modulation of iron reduction potential by deprotonation at a remote site. Chem Commun. 1998;24:2681–2.
77. Brewer C, Brewer G, Luckett C, Marbury GS, Viragh C, Beatty AM, Scheidt RW. Proton control of oxidation and spin state in a series of iron tripodal imidazole complexes. Inorg Chem. 2004;43:2402–15.
78. Lambert F, Policar C, Durot S, Cesario M, Yuwei L, Korri-Youssoufi H, Keita B, Nadjo L. Imidazole and imidazolate iron complexes: on the way for tuning 3D-structural characteristics and reactivity. Redox interconversions controlled by protonation state. Inorg Chem. 2004;43:4178–88.
79. Anxolabéhère-Mallart E, Costentin C, Policar C, Robert C, Savéant J-M, Teillout A-L. Proton-coupled electron transfers in biomimetic water bound metal complexes. The electrochemical approach. Faraday Discuss. 2011;48:83–95.
80. Vallee BL, Williams RJP. Metalloenzymes-entatic nature of their active sites. Proc Natl Acad Sci U S A. 1968;59(2):498–505.
81. Jahn HA, Teller E. Stability of polyatomic molecules in degenerate electronic states. I. Orbital degeneracy. Proc R Soc London Ser A. 1937;161(A905):220–35.
82. Deeth RJ. The ligand field molecular mechanics model and the stereoelectronic effects of d and s electrons. Coord Chem Rev. 2001;212:11–34.
83. Koppenol WH. The physiological role of charge distribution on SOD. In: Rodgers MAJ, editor. Oxygen and oxy-radicals in chemistry and biology. New York: Academic; 1981. p. 671–4.
84. Benovic J, Tillman T, Cudd A, Fridovich I. Electrostatic facilitation of the reaction catalyzed by the manganese-containing and iron-containing SOD. Arch Biochem Biophys. 1983;221:329–32.
85. Getzoff ED, Tainer JA, Weiner PK, Kollman PA, Richardson JS, Richardson DC. Electrostatic recognition between superoxide and copper-zinc SOD. Nature. 1983;306:287–90.
86. Sines J, Allison S, Wierzbicki A, McCammon JA. Brownian dynamics simulation of the superoxide-superoxide dismutase reaction: iron and manganese enzymes. J Phys Chem. 1990;94:959–61.
87. Cudd A, Fridovich I. Electrostatic interactions in the reaction mechanism of bovine Erythrocyte superoxide dismutase. J Biol Chem. 1982;257:11443–7.
88. Allison SA, Bacquet RJ, McCammon JA. Simulation of the diffusion-controlled reaction between superoxide and superoxide dismutase. II. Detailed models. Biopolymers. 1988;27:251–69.
89. Parker MW, Blake CCF. Crystal structure of MnSOD from Bacillus stearothermopilus at 2.4 Å resolution. J Mol Biol. 1988;199(2):649–61.
90. Wispe JR, Clark JC, Burhans MS, Kropp KE, Korfhagen TR, Whitsett JA. Synthesis and processing of the precursor for human mangano-superoxide dismutase. Biochim Biophys Acta. 1989;994:30–6.
91. Durand G, Polidori A, Pucci B. La vectorisation de pièges à radicaux libres. Nouvelle stratégie thérapeutique. Act Chimique. 2003;26–29.

92. Favier A. Le stress oxydant. Intérêt conceptuel et expérimental dans la compréhension des mécanismes des maladies et potentiel thérapeutique. Act Chimique. 2003;11–12:108–15.
93. Smith AJ, Porteous CM, Gane AM, Murphy MP. Delivery of active molecules to mitochondria *in vivo*. Proc Natl Acad Sci U S A. 2003;100:5407–12.
94. Dhanasekaran A, Kotamraju S, Karunakaran C, Kalivendi SV, Thomas S, Joseph J, Kalyanaraman B. Mitochondria superoxide dismutase mimetic inhibits peroxide-induced oxidative damage and apoptosis: role of mitochondrial superoxide. Free Radical Biol Med. 2005;39:567–83.
95. Rafelski S. Mitochondrial network morphology: building an integrative, geometrical view. BMC Biol. 2013;11:71.
96. Fernandez-Carneado J, van Gool M, MMartos V, Castel S, Prados P, de Mendoza J, Giralt E. Highly efficient, nonpeptidic oligoguanidinium vectors that selectively internalize into mitochondria. J Am Chem Soc. 2005;127:869–74.
97. Policar C, Durot S, Lambert F, Cesario M, Ramiandrasoa F, Morgenstern-Badarau I. New Mn(II) complexes with N/O coordination sphere from tripodal N-centered ligands. Characterization from solid state to solution and reaction with superoxide in non-aqueous and aqueous medium. Eur J Inorg Chem. 2001;1807–18.
98. Dees A, Zahl A, Puchta R, van Eikema Hommes NJR, Heinemann FW, Ivanovic-Burmazovic I. Water exchange on seven-coordinate Mn(II) complexes with macrocyclic pentadentate ligands: insight in the mechanism of Mn(II) SOD-mimetic. Inorg Chem. 2007;46:2459–70.
99. Salvemini D, Wang Z-Q, Zweier JL, Samouilov A, Macarthur H, Misko TP, Currie MG, Cuzzocrea S, Sikorski JA, Riley DP. A non-peptidyl mimic of SOD with therapeutic activity in rats. Science. 1999;286:304–5.
100. Xingcan S, Hong L, Zhiliang J, Xiwen H, Panwen P. Binding equilibrium study between Mn(II) and HSA or BSA. Chin J Chem. 2000;18(1):35–41.
101. Munroe W, Kingsley C, Durazo A, Butler Gralla E, Imlay JA, Srinivasan C, Valentine JS. Only one of a wide assortment of manganese-containing SOD mimicking compounds rescues the slow aerobic growth phenotypes of both Escherichia coli and Saccharomyces cerevisiae strains lacking superoxide dismutase enzymes. J Inorg Biochem. 2007; 101:1875–82.
102. Spasojevic I, Chen Y, Noel TJ, Yu Y, Cole MP, Zhang L, Zhao Y, St. Clair DK, Batinic-Haberle I. Mn-porphyrin-based superoxide dismutase mimic, [Mn(III)TE2PyP]5+ target mouse heart mitochondria. Free Radical Biol Med. 2007;42:1193–200.
103. Clède S, Lambert F, Saint-Fort R, Plamont MA, Bertrand H, Vessières A, Policar C. Influence of the side-chain length on the cellular uptake and the cytotoxicity of rhenium triscarbonyl derivatives: a bimodal infrared and luminescence quantitative study. Chem Eur J. 2014;20:8714–22.
104. Policar C, Lambert F, Cesario M, Morgenstern-Bararau I. An inorganic helix [Mn(IPG)(MeOH)]n[PF6]n: structural and magnetic properties of a syn-anti carboxylate-bridged manganese(II) chain involving a tetradentate ligand. Eur J Inorg Chem. 1999; (12):2201–7.
105. Cisnetti F, Lefevre AS, Guillot R, Lambert F, Blain G, Anxolabéhère-Mallart E, Policar C. A new pentadentate ligands forms both a di- and mononuclear Mn(II) complex: electrochemical, spectroscopic and SOD activity studies. Eur J Inorg Chem. 2007;4472–80.
106. Cisnetti F, Pelosi G, Policar C. Synthesis and superoxide dismutase-like activity of new manganese(III) complexes based on tridentate N2O ligands derived from histamine. Inorg Chim Acta. 2007;360:557–62.
107. Groni S, Blain G, Guillot R, Policar C, Anxolabéhère-Mallart E. Reactivity of Mn(II) with superoxide. Evidence for a [$Mn^{III}OO$]+ unit by low-temperature spectroscopies. Inorg Chem. 2007;46:1951–3.
108. Bernard A-S, Giroud C, Ching HYV, Meunier A, Ambike V, Amatore C, Guille Collignon M, Lemaître F, Policar C. Evaluation of the anti-oxidant properties of a SOD-mimic Mn-complex in activated macrophages. Dalton Trans. 2012;41:6399–403.

109. Borgstahl GOE, Parge HE, Hickey MJ, Beyer WF, Hallewell RA, Tainer JA. The structure of human mitochondrial manganese superoxide dismutase reveals a novel tetrameric interface of two 4-helix bundles. Cell. 1992;71:107–18.
110. Tabares LC, Cortez N, Hiraoka BY, Yamakura F, Un S. Effects of substrate analogues and pH on manganese superoxide dismutases. Biochemistry. 2006;45(6):1919–29.
111. Whittaker MM, Whittaker JW. Low-temperature thermochromism marks a change in coordination for the metal ion in manganese superoxide dismutase. Biochemistry. 1996;35(21): 6762–70.
112. Yamato K, Miyahara I, Ichimura A, Hirotsu K, Kojima Y, Sakurai H, Shiomi D, Sato K, Takui T. Superoxide dismutase mimetic complex of Mn(II)/N, N-bis(2-pyridylmethyl)-(S)-histidine. Chem Lett. 1999;28:295–6.
113. Nishida Y, Tanaka N, Yamazaki A, Tokii T, Hashimoto N, Ide K, Iwasawa K. Novel reactivity of dioxygen molecule in the presence of Mn(II) complex and reducing agents. Inorg Chem. 1995;34:3616–20.
114. Ching HYV, Anxolabehere-Mallart E, Colmer HE, Costentin C, Dorlet P, Jackson TA, Policar C, Robert M. Electrochemical formation and reactivity of a manganese peroxo complex: acid driven H_2O_2 generation vs. O-O bond cleavage. Chem Sci. 2014;5(6):2304–10.
115. Kitajima N, Komatsuzaki H, Hikichi S, Osawa M, Moro-Oka Y. A monomeric side-on peroxo Mn(III) complex: $Mn(O_2)(3,5\text{-}iPr_2pzH)(HB(3,5\text{-}iPr_2pz))$. J Am Chem Soc. 1994; 116:11596–7.
116. Primus J-L, Grunenwald S, Hagedoorn P-L, Albrecht-Gary A-M, Mandon D, Veeger C. The nature of the intermediates in the reaction of Fe(III) and Mn(III)-microperoxidase 8 with H_2O_2: a rapid kinetics study. J Am Chem Soc. 2002;124(7):1214–21.
117. Seo MS, Kim JY, Annaraj J, Kim Y, Lee Y-M, Kim S-J, Kim J, Nam W. [Mn(tmc)(O2)]+: a side-on peroxido manganese(III) complex bearing a non-heme ligand. Angew Chem Int Ed Engl. 2007;46:377–80.
118. Groni S, Dorlet P, Blain G, Bourcier S, Guillot R, Anxolabehere-Mallart E. Reactivity of an aminopyridine LMn^{II} complex with H_2O_2. Detection of intermediates at low temperature. Inorg Chem. 2008;47(8):3166–72.
119. Leto DF, Chattopadhyay S, Daya VW, Jackson TA. Reaction landscape of a pentadentate N5-ligated MnII complex with $O_2^{\bullet-}$ and H_2O_2 includes conversion of a peroxomanganese(III) adduct to a bis(μ-oxo)-dimanganese(III, IV) species. Dalton Trans. 2013;42:13014–25.
120. Enemark JH, Feltham RD. Principles of structure, bonding, and reactivity for metal nitrosyl complexes. Coord Chem Rev. 1974;13(4):339–406.
121. Bielski BHJ, Arudi RL. Preparation and stabilization of aqueous/ethanolic superoxide solutions. Anal Biochem. 1983;133:170–8.
122. Bielski BHJ. Reevaluation of the spectral and kinetic properties of HO_2 and O_2^- free radicals. Photochem Photobiol. 1978;28:645–9.
123. Cabelli DE, Bielski BHJ. Pulse radiolysis study of the kinetics and mechanisms of the reaction between Mn(II) complex and HO_2/O_2- radicals. 1. sulfate, formate and pyrophosphate complexes. J Phys Chem. 1984;88(14):3111–5.
124. Cabelli D. Probing superoxide dismutases through radiation chemistry. Isr J Chem. 2014;54(3):272–8.
125. Friedel FC, Lieb D, Ivanovic-Burmazovic I. Comparative studies on manganese-based SOD mimetics, including the phosphate effect, by using global spectral analysis. J Inorg Biochem. 2012;109:26–32.
126. Batinic-Haberle I, Spasojevic I, Hambright P, Benov L, Crumbliss AL, Fridovich I. Relationship among redox potentials, proton dissociation constants of pyrrolic nitrogens and in vivo SOD activities of Mn(III) and iron(III) water soluble porphyrins. Inorg Chem. 1999;38:4011–22.
127. Okado-Matsumoto A, Batinic-Haberle I, Fridovich I. Complementation of SOD-deficient Escherichia coli by manganese porphyrin mimics of superoxide dismutase activity. Free Radical Biol Med. 2004;37(3):401–10.

128. Tovmasyan A, Carballal S, Ghazaryan R, Melikyan L, Weitner T, Maia CGC, Reboucas JS, Radi R, Spasojevic I, Benov L, Batinic-Haberle I. Rational design of superoxide dismutase (SOD) mimics: the evaluation of the therapeutic potential of New cationic Mn porphyrins with linear and cyclic substituents. Inorg Chem. 2014;53(21):11467–83.
129. Ndengele MM, Muscoli C, Zhi QW, Doyle TM, Matuschak GM, Salvemini D. Superoxide potentiates NF-kappa B activation and modulates endotoxin-induced cytokine production in alveolar macrophages. Shock. 2005;23(2):186–93.
130. Asayama S, Kawamura E, Nagaoaka S, Kawakami H. Design of Mn-porphyrin modified with a mitochondrial signal peptide for a new antioxidant. Mol Pharm. 2006;3:468–70.
131. Amatore C, Arbault S, Guille M, Lemaitre F. Electrochemical monitoring of single cell secretion: vesicular exocytosis and oxidative stress. Chem Rev. 2008;108:2585–621.
132. Lewis EA, Lindsay-Smith JR, Walton PH, Archibald SJ, Foxo SP, Giblin GMP. Tuning the metal-based redox potential of manganese cis, cis-1,3,5-triaminocyclohexane complexes. J Chem Soc Dalton Trans. 2001;1159–61.
133. Lewis EA, Khodr HH, Hider RC, Lindsay-Smith JR, Walton PH. A manganese superoxide dismutase mimic based on cis-cis-1,3,5-triaminocyclohexane. Dalton Trans. 2004;2:187–8.
134. Collman J. Synthetic models for the oxygen-binding hemoproteins. Acc Chem Res. 1977;10:265–72.
135. Momenteau M. Synthesis and coordination properties of superstructure iron-porphyrins. Pure Appl Chem. 1986;58(11):1493–502.
136. Collman J, Fu L. Synthetic models for hemoglobin and myoglobin. Acc Chem Res. 1999;32:455–63.
137. Collman J, Ghosh S. Recent applications of synthetic model of cytochrome c oxidase: beyond functional modeling. Inorg Chem. 2010;49:5798–810.
138. Batinic-Haberle I, Benov L, Spasojevic I, Fridovich I. The ortho effect makes Mn(III)porphyrins a powerful potentially used SOD mimic. J Biol Chem. 1998;273(38):24521–8.
139. Batinic-Haberle I, Spasojevic I, Stevens RD, Hambright P, Neta P, Okado-Matsumoto A, Fridovich I. New class of potent catalysts of superoxide dismutation. Mn(III) ortho-methoxyethylpyridyl- and di-ortho-methoxyethyl-imidazolylporphyrins. Dalton Trans. 2004; 11:1696–702.
140. Maroz A, Kelso GF, Smith RAJ, Ware DC, Anderson RF. Pulse radiolysis investigation on the mechanism of the catalytic action of Mn(II)—Pentaazamacrocycle compounds as superoxide dismutase mimetics. J Phys Chem A. 2008;112(22):4929–35.
141. Batinic-Haberle I, Liochev SI, Spasojevic I, Fridovich I. A potent SOD mimic: Mnßoctabromo meso tetrakis(Npyridinium4yl)porphyrin. Arch Biochem Biophys. 1997;343(2):225–33.
142. Spasojević I, Batinic-Haberle I, Rebouças JS, Idemori YM, Fridovich I. Electrostatic Contribution in the catalysis of superoxide dismutation by SOD mimics. J Biol Chem. 2003; 278:6831–7.
143. Rajic Z, Tovmasyan A, Spasojevic I, Sheng H, Lu M, Li A-M, Batinic-Haberle I, Benov LT. A new SOD mimic, Mn(III) ortho N-butoxyethylpyridylporphyrin, combines superb potency and lipophilicity with low toxicity. Free Radical Biol Med. 2012;52:1828–34.
144. Rebouças JS, DeFreitas-Silva G, Spasojević I, Idemori YM, Benov L, Batinić-Haberle I. Impact of electrostatics in redox modulation of oxidative stress by Mn porphyrins: Protection of SOD-deficient Escherichia coli via alternative mechanism where Mn porphyrin acts as a Mn carrier. Free Radical Biol Med. 2008;45:201–10.
145. Friedel FC, Kenkell I, Miljkovic JL, Moldenhauer D, Weber N, Filipovic ML, Gröhn F, Ivanovic-Burmazovic I. Amphiphilic pentaazamacrocyclic manganese superoxide dismutase mimetics. Inorg Chem. 2014;53:1009–20.
146. Puglisi A, Tabb G, Vecchio G. Bioconjugates of cyclodextrins of manganese salen-type with superoxide dismutase activity. J Inorg Biochem. 2004;98:969–76.
147. Rebouças JS, Spasojevic I, Tjahjono DH, Richaud A, Méndez F, Benov L, Batinic-Haberle I. Redox modulation of oxidative stress by Mn porphyrin-based therapeutics: the effect of charge distribution. Dalton Trans. 2008;9:1233–42.

148. Asayama S, Hanawa T, Nagaoka S, Kawakami H. Design of the complex between manganese porphyrins and catalase-poly(ethylene glycol) conjugates for a new antioxidant. Mol Pharm. 2007;4(3):484–6.
149. Hanawa T, Asayama S, Watanabe T, Owada S, Kawakami H. Protective effects of the complex between manganese porphyrins and catalase-poly(ethylene glycol) conjugates against hepatic ischemia/reperfusion injury in vivo. J Controlled Release. 2009;135(1):60–4.
150. D'agata R, Grasso G, Iacono G, Spoto G, Vecchio G. Lectin recognition of a new SOD mimic bioconjugate studied with surface plasmon resonance imaging. Org Biomol Chem. 2006;4:610–2.
151. Asayama S, Mizushima K, Nagaoka S, Kawakami H. Design of metalloporphyrin-carbohydrate conjugates for a New superoxide dismutase mimic with cellular recognition. Bioconjugate Chem. 2004;15:1360–3.
152. Kelso GF, Maroz A, Cocheme HM, Logan A, Prime TA, Peskin AV, Winterbourn CC, James AM, Ross MF, Brooker S, Porteous CM, Anderson RF, Murphy MP, Smith RAJ. A mitochondria-targeted macrocyclic Mn(II) superoxide dismutase mimetic. Chem Biol. 2012;19(10): 1237–46.
153. Aitken JB, Shearer EL, Giles NM, Lai B, Vogt S, Reboucas JS, Batinic-Haberle I, Lay PA, Giles GI. Intracellular targeting and pharmacological activity of the SOD mimics MnTE-2-PyP(5+) and MnTnHex-2-PyP(5+) regulated by their porphyrin ring substituents. Inorg Chem. 2013;52:4121–3.
154. Fridovich I. Quantitative aspects of the production of superoxide anion radical by milk xanthine oxidase. J Biol Chem. 1970;245(16):4053–7.
155. Castello PR, Drechsel DA, Day BJ, Patel M. Inhibition of mitochondrial hydrogen peroxide production by lipophilic metalloporphyrins. J Pharmacol Exp Ther. 2008;324:970–6.
156. Okado-Matsumoto A, Fridovich I. Assay of superoxide dismutase: cautions relevant to the use of cytochrome c, a sulfonated tetrazolium, and cyanide. Anal Biochem. 2001; 298:337–42.
157. Pasternack RF, Halliwell B. Superoxide dismutase activities of an iron porphyrin and other iron complexes. J Am Chem Soc. 1979;101(4):1026–31.
158. Butler J, Koppenol WH, Margoliash E. Kinetics and mechanism of the reduction of ferricytochrome c by the superoxide anion. J Biol Chem. 1982;257(18):10747–50.
159. Liao Z-R, Zheng X-F, Luo B-S, Shen L-R, Li D-F, Liu H-L, Zhao W. Synthesis, characterization and SOD-like activities of manganese-containing complexes with N, N, N′, N′-tetrakis(2′-benzimidazolyl methyl)-1,2-ethanediamine (EDTB). Polyhedron. 2001;20:2813–21.
160. Weiss RH, Flickinger AG, Rivers WJ, Hardy MM, Aston KW, Ryan US, Riley DP. Evaluation of activity of putative superoxide dismutase mimics. Direct analysis by stopped-flow kinetics. J Biol Chem. 1993;268(31):23049–54.
161. Faulkner KM, Liochev SI, Fridovich I. Stable Mn(III) porphyrins mimic SOD in vitro and substitute for it in vivo. J Biol Chem. 1994;269(38):23471–6.
162. Note that after 10 min. the concentration in dioxygen drops too much and the OD as a function of time is no longer linear.
163. Spasojevic I, Batinic-Haberle I, Stevens RD, Hambright P, Thorpe AN, Grodkowski J, Neta P, Fridovich I. Mn(III) biliverdin IX dimethylester: a powerful catalytic scavenger of superoxide employing the Mn(III)/Mn(IV) redox couple. Inorg Chem. 2001;40:726–39.
164. Liochev SI, Fridovich I. Superoxide from glucose oxidase or from nitroblue tetrazolium? Arch Biochem Biophys. 1995;318:408–10.
165. Batinic-Haberle I, Rebouças Julio S, Spasojevic I. Response to Rosenthal et al. Antiox redox signal. 2011;14(6):1174–6.
166. Bull C, McClune GJ, Fee JA. The mechanism of Fe-EDTA catalysed superoxide dismutation. J Am Chem Soc. 1983;103:5290–300.
167. Riley DP, Rivers WJ, Weiss RH. Stopped-flow kinetic analysis for monitoring SO decay in aqueous systems. Anal Biochem. 1991;196:344–9.
168. Ching HYV, Kenkel I, Delsuc N, Mathieu E, Ivanović-Burmazovic I and Policar C, Bioinspired superoxide-dismutase mimics: The effects of functionalization with cationic polyarginine peptides. J Inorg Biochem. 2016;160:172–9.